European Commission Grant Agreement Number: 869300

Call identifier: H2020-LC-CLA-2018-2019-2020 Topic: LC-CLA-06-2019

Type of action: RIA, Research and Innovation action

Starting date: 01.09.2020 Duration: 48 months

Project website: futuremares.eu

Project Deliverable Report

Report on hindcast and projection uncertainty in physical biogeochemical simulations across all regions as well as description of the model scenarios (climate scenarios), and combination into an ensemble.

Dissemination level: **Public**

Type of deliverable: Report

Due date: Project month 26 [30.10.2022]

Project Milestone(s) achieved:
None of relevant

FutureMARES Project

FutureMARES - Climate Change and Future Marine Ecosystem Services and Biodiversity is an EU-funded research project examining the relations between climate change, marine biodiversity and ecosystem services. Our activities are designed around two Nature-based Solutions (NBS1 habitat restoration, NBS2 conservation) as well as Nature-inclusive (sustainable) Harvesting (NIH).

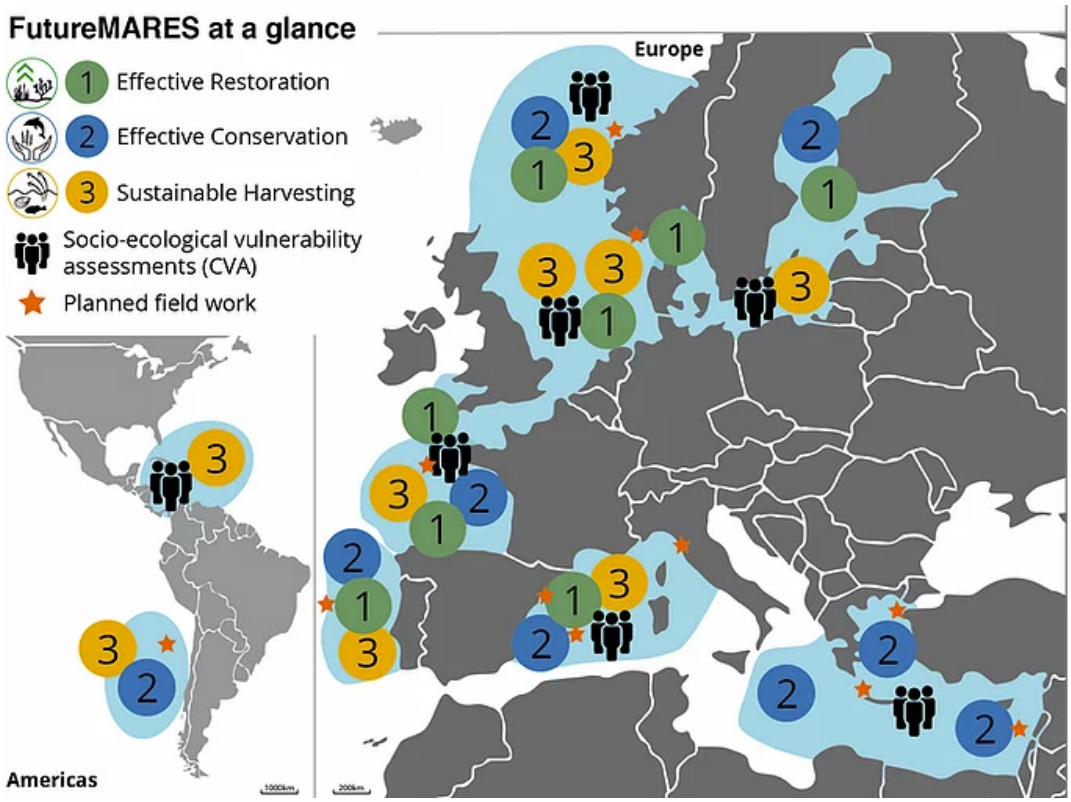

We are conducting our research and cooperating with marine organisations and the public in Case Study Regions across Europe and Central and South America. Our goal is to provide science-based policy advice on how best to use NBS to protect future biodiversity and ecosystem services in a future climate.

FutureMARES provides socially and economically viable actions and strategies in support of nature-based solutions for climate change adaptation and mitigation. We develop these solutions to safeguard future biodiversity and ecosystem functions to maximise natural capital and its delivery of services from marine and transitional ecosystems. To achieve this, the objectives of FutureMARES defined following goals:

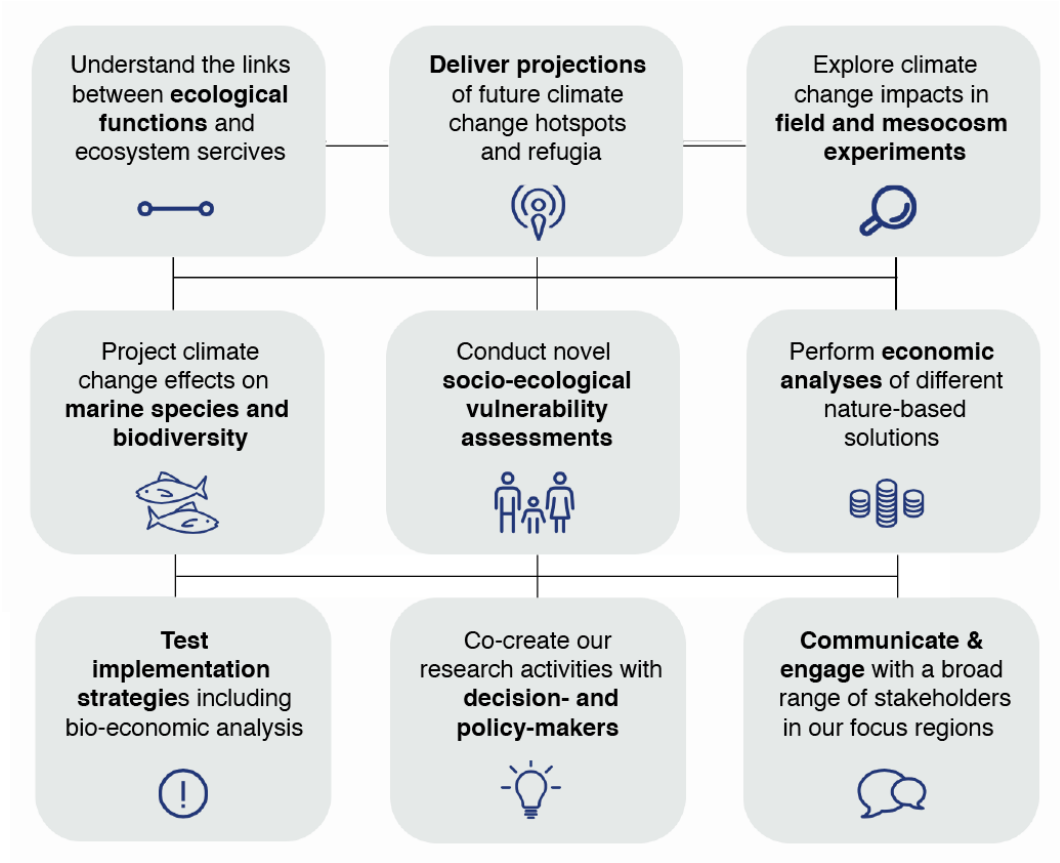
Understand the links between **ecological functions** and ecosystem sercives
Deliver projections of future climate change hotspots and refugia
Explore climate change impacts in **field and mesocosm experiments**
Project climate change effects on **marine species and biodiversity**
Conduct novel **socio-ecological vulnerability assessments**
Perform **economic analyses** of different nature-based solutions
Test implementation strategies including bio-economic analysis
Co-create our research activities with **decision- and policy-makers**
Communicate & engage with a broad range of stakeholders in our focus regions

Deliverable data	
Work Package(s) / Task(s):	WP2 – Changing Habitats
Lead beneficiary:	CMCC
Responsible author:	Momme Butenschön
Contact:	momme.butenschon@cmcc.it
Co-authors:	Trond Kristiansen
Date of delivery:	16/03/2023
Deliverable type:	Report
Date of internal approval (for the submission to EC)	16/03/2023

Involved partners

Project partner (affiliation)	First name	Last name	E-mail
CMCC	Momme	Butenschön	momme.butenschon@cmcc.it
NIVA	Trond	Kristiansen	

Document history

Version	**Date**	**Description**
01	13.03.23	V1.0 – Initial version by Author (Momme Butenschön)
02	13.03.23	V1.1 – Reviewed by Scientific Coordinator (Myron Peck)
03	15.03.23	V1.2 – Reviewed by Author (Momme Butenschön)

Suggested citation for this report: Butenschön, M. and Kristiansen, T. ([2023]) *[Report on hindcast and projection uncertainty in physical biogeochemical simulations across all regions as well as description of the model scenarios (climate scenarios), and combination into an ensemble.]* FutureMARES Project Deliverable report

FutureMARES receives funding from the European Union's Horizon 2020 research and innovation programme under grant agreement No 869300 "Climate Change and Future Marine Ecosystem Services and Biodiversity"

Table of content

Table of Contents

List of symbols, abbreviations and a glossary

BA	Bias Adjustment
CC	Climate change
CM	Climate Model
CMIP	Coupled Model Intercomparison Project
CORDEX	Coordinated Regional Downscaling Experiment
DoA	Description of Action, a part of the project Grant Agreement describing the project work plan
EC	European Commission
EC GA	European Commission Grant Agreement – a contract between the European Commission and FutureMARES consortium
ESM	Earth System Model
GA	Grant Agreement
IPCC	Intergovernmental Panel on Climate Change
MIP	Model Intercomparison Project
NBS	Nature-based Solutions
NIH	Nature-inclusive (sustainable) Harvesting
RCP	Representative Concentration Pathway
SD	Statistical Downscaling
SSP	Shared Socioeconomic Pathway
Tn.x	Task – an sub-component of a work package where “n” is a number of the work package and “x” is a number of the task within this work package
WP	Work Package

Executive Summary

This report presents an updated version of the Statistical Downscaling Ensemble for the Regional Seas of FutureMARES, a quantitative evaluation of its performance against observations compared to the performance of the original Climate and Earth System Models from the CMIP6 archives and an assessment of the uncertainties attached to the future projections investigating three sources of uncertainty: internal variability, model uncertainty and scenario uncertainty.

The ensemble provides datasets for 5 different indicators of the marine habitat conditions (temperature, salinity, pH, dissolved oxygen, chlorophyll) at three distinct depth levels (surface, sub-surfaces and seafloor) for the years 1993 – 2100 under three different future scenarios. It is produced via bias adjustment and statistical downscaling of 4-6 individual Climate or Earth System Models, depending on the variable, and provides projections for three different pathways of greenhouse gas emissions, Global Sustainability (SSP1-2.6), Middle of the Road (SSP2-4.5) and World Markets SSP5-8.5.

Validation of the ensemble against observations (CORA v2.5 dataset) and observation based climatologies (World Ocean Atlas) show that model bias has been successfully removed across all quantiles, the ensemble faithfully represents the present state of the system and its variability reducing inter-model differences significantly.

The future projections of the ensemble qualitatively resemble the trajectories of the global simulations at basin average except from the Baltic Sea which is much more affected by local, coastal processes than the other regions, leading to significant uncertainties in the projections. Warming is evident across all regions, even if it fully emerges from the background uncertainties related to internal variability and model differences only in the second half of the century with substantial difference in between the greenhouse gas emission trajectories. Acidification has significantly emerged from model uncertainty and internal variability already at present day, while the different scenarios lead to distinct trajectories in surface pH starting from little earlier than mid-century. Deoxygenation appears to be present across all domains, but the signal is significantly weaker compared to the other two pressures when compared to model uncertainty and internal variability and the impact of different greenhouse gas trajectories is much less distinct.

It should be noted however, that these qualitative characteristics vary considerably in extent and show substantial local heterogeneity within each domain underlining the importance of a spatially explicit and well resolved approach to address the question of impacts of anthropogenic climate change on the marine ecosystem functions and services.

Contribution to the project

The ensemble, originally presented and published in D2.1, and its subsequent assessment and analysis provides the physical and biogeochemical science basis depicting the changing habitat condition in response to anthropogenic green-house gas emissions for the FutureMARES Storylines. The particular strength of this contribution with respect to existing datasets is to provide information on the extent and uncertainty of environmental change at scales that are relevant and accessible for the problems addressed by the Storylines of this project aiming to support the local to regional management of ecosystem services related to

the Nature-based Solutions (NBS) and the Nature-inclusive Harvesting (NIH) addressed in FutureMARES.

This report provides an updated and much extended version of the basic report accompanying the release of the first version of the ensemble dataset. It includes a detailed description of the statistically downscaled regional ensemble of physical and biogeochemical habitat conditions for the regions of interest of the FutureMARES project with a natural focus on the European Seas. It also assesses its performance against observations and explores and documents the uncertainties in the projections.

Dissemination and Exploitation

The ensemble dataset and the information on the extent of physical and biogeochemical changes in marine and coastal habitats derived from it, along with uncertainty estimates, has been distributed to all project partners. These projections provide a basis for much of the scenario explorations performed in FutureMARES, particularly the single-species to ecosystem models projections of the impacts of scenarios of NBS and/or NIH implementation (WP4), as well as the downstream spatial, bioeconomic and/or Bayesian statistical analyses (WP6.1, 6.2 and 6.3). The first version of the underlying datasets was published Open Access for non-commercial use with D2.1 in May 2022. In the following 9 months, it has been viewed and downloaded several hundreds of times. Further iterations and additions to the datasets have been made available internally to project partners and will be made publicly available upon publication of a manuscript that is currently under preparation based on the contents of D2.1 and the analysis presented in this report.

1. Introduction

Climate and Earth System Models (CMs and ESMs) are used as a primary means to understand how habitat conditions have changed in the past and are expected to change in the future due to a range of scenarios of anthropogenic green-house gas emissions. These models are complex tools that can simultaneously model the physics, chemistry, and biology of land, ocean, atmosphere, and cryosphere allowing researchers to explore the intricate relationships and dependence of these earth systems. An important part of the IPCC Assessment reports (IPCC, 2021) is the analysis of output from the Coupled Model Intercomparison Project (CMIP) which simulates future climate using the described Shared Socioeconomic Pathways (SSP) narratives and Representative Concentration Pathways (RCPs) of future emissions. The CMIP models are global in scope and cover the atmosphere, land, and ocean. They provide a wealth of invaluable, broad information at large spatial scales illustrating the evolution of the mean state of the Earth System and, importantly, the uncertainties involved in the model projections. In fact, an important characteristic of the CMIP approach is the standardised sets of experiments (the so-called MIPS) based on well-defined protocols and supported and applied by a large international modelling community.

The relatively coarse-scale resolution of these CMIP models (most are 1x1-degree longitude-latitude in the ocean for the current CMIP6 generation of models) does not adequately resolve details of the regional and coastal domains of marine habitats that are increasingly required for the strategic planning and management of marine resources and ecosystem services as well as for the development of climate change adaptation and mitigation policies. Addressing of these shortcomings clearly requires the downscaling of the global datasets in order to obtain dataset at adequate resolutions that are consistent with the large-scale information from the ESM and CM projections.

While a significant number of individual dynamical downscaling products exist for regional ocean domains, these lack the conceptual and standardised approach of the CMIP experiments or the CORDEX experiments available for regional atmospheric domains. Dynamic downscaled products also lack the broadness of the global datasets in terms of experiment realisations. This strongly limits the comparability of results among different systems and does not adequately quantify the uncertainties involved in the projections (Drenkard et al., 2021).

To overcome these shortcomings, we applied a statistical bias-correction (BA) and downscaling (SD) of the global CMIP6 projections. The BA corrects systematic errors in the climate data to minimize the errors between observed and modelled values for a specific control period, while the SD allows us to establish an empirical relationship between historical fine-scale data and large-scale climate variables and applies this statistical connection to project future climate at smaller (local) scales. This approach produces a high-resolution climate dataset using a range of CMIP6 models and ensemble members (realizations) containing both the historical (1993-2020) and future projections (2021-2100) that captures the uncertainty across models. This document provides a detailed description of the ensemble dataset, the approaches that were taken to build it, an assessment of its performance, and underlying uncertainties of these projections.

2. Methodology

2.1. Downscaling and Bias Correction

2.1.1 Preparation of global climate data

The raw global climate models (GCMs) and Earth System Models (ESMs) can be represented on a variety of grids covering the globe. Some of these grids have higher resolution in one part of the world, e.g., around the equator, while others can have 2 north poles and 1 south pole to avoid the singularity of the north pole at 90N. To be able to work consistently with these model outputs, we interpolated the data to a uniform cartesian grid of 0.5 x 0.5-degree longitude-latitude. This interpolation was done using the Earth System Modelling Framework (ESMF) to allow for fast interpolation in a tested framework. We also used the Python xesmf interface to the ESMF package which further simplifies the conversion from the native grid to a uniform grid. Once the GCM/ESM data were converted to the standard grid, we performed a bias-corrected statistical downscaling of the data including two steps: 1) bias-correction and 2) statistical downscaling.

2.1.2 Bias correction

CMs and ESMs are inherently biased from historical observations as they focus on efficient representations of large-scale processes and feedbacks at the Earth System interfaces rather than regional and local fidelity. Rather, the CMs and ESMs represent the probability distributions of physical and biological variables, their variability, and the long-term trends as observed. To correct this offset in the global models, we performed a bias-correction where the large-scale climate signal was constrained to the historical ranges by using detrended quantile mapping transformation removing bias across the entire spectrum of the model distributions. The bias-correction removed systematic errors in the climate data to minimise the errors between observed and modelled values for a specific control period. This bias-correction was performed at the resolution of a standardised 0.5 x 0.5-degree latitude-longitude grid.

In addition, it should be noted that CMs and ESMs are spun-up over centuries to reach the internal model equilibrium and sent off uninitialized in the production runs starting at preindustrial age. This is done to avoid long-term drifts in the energy and biogeochemical budgets and trustworthy represent long-term trends in the natural system. Therefore, they cannot be expected to match historical interannual variability in phase and should not be used in the context of short-term predictions or forecasts.

2.1.3 Statistical downscaling

Statistical downscaling allows us to establish an empirical relationship between historical and large-scale climate variables and to apply these statistics to project future climate at local scales. The bias-corrected fields at 0.5 x 0.5 degrees longitude-latitude resolution are used as input to the statistical downscaling algorithm which is a detrended quantile mapping transformation onto a high-resolution historical reanalysis. The reanalysis used is GLORYS12V11 from Mercator Ocean, an operational service from the Copernicus Marine Service Center (marine.copernicus.eu). The global ocean physics is well represented in the GLORYS12V1 reanalysis, at 1/12th degrees resolution, and has been thoroughly validated against observations (Drévillon et al., 2022). The GLORYS12V1 reanalysis assimilates available historical data (e.g., satellite, CTD, XBT, buoys) for the period

1993-2020, and represents state-of-the-art hydrodynamic biogeochemical modelling. The temporary period covered by the reanalysis is from January 1993 to December 2019. The model has 50 vertical depth levels which were linearly interpolated if downscaling was performed at an intermediate depth level. A linear interpolation was also performed on the global climate model outputs as downscaling was done at individual fixed depth levels. An exception was the bottom, where each grid point had a unique depth level.

The downscaling was performed on anomalies rather than actual values. The anomalies were obtained from both the GLORYS data and the CMIP6 climate data by removing the detrended monthly climatology. This removal of the seasonality allowed a much bigger dataset (and therefore statistical coverage) to be generated over the historical time period which was used to train the downscaling algorithm (324 data points per grid point). Once the downscaling was completed, we added the detrended GLORYS climatology which preserved the trend from the CMIP6 model. This approach is different from typical atmospheric downscaling which is often performed on a monthly basis due to the daily frequency of data, providing a much larger dataset to be used for training of the downscaling (see e.g., ISIMIP3BASD).

Historical biological observations such as oxygen, chlorophyll, and pH were obtained from the biological model Global Ocean Biogeochemistry hindcast (GOBH) from Mercator Ocean for oxygen and chlorophyll. The GOBH model used the PISCES model to represent biogeochemistry and a non-assimilative version of GLORYS for physics (Perruche et al., 2019). The GOBH model had a slightly coarser resolution of 1/4th degrees. To be able to directly compare the downscaled physical and biological results, we interpolated and extrapolated the biological model data onto the grid of the physical model, allowing us to deliver biological downscaled data at 1/12th degree resolution.

2.1.4 Final product

Once the downscaling was finished, the results were stored as NetCDF4 files which contain self-describing metadata of the downscaled variable. We also stored the bottom depth matrix for easy filtering of data based on maximum depth. The downscaling was performed for a range of CMIP6 models (4-6) per variable per climate scenario (see Table 1) at three discrete depths corresponding to surface (5m), subsurface (25m) and seafloor, and the final product to be used by researchers is an ensemble of these individual downscaled models.

2.2. Domains

The domains of the European Seas over which the statistical downscaling was applied is depicted in Figure 1. They contain all major basins and shelf seas of the European continent except for the Black Sea and cover all FutureMARES Storylines located across European coasts and seas.

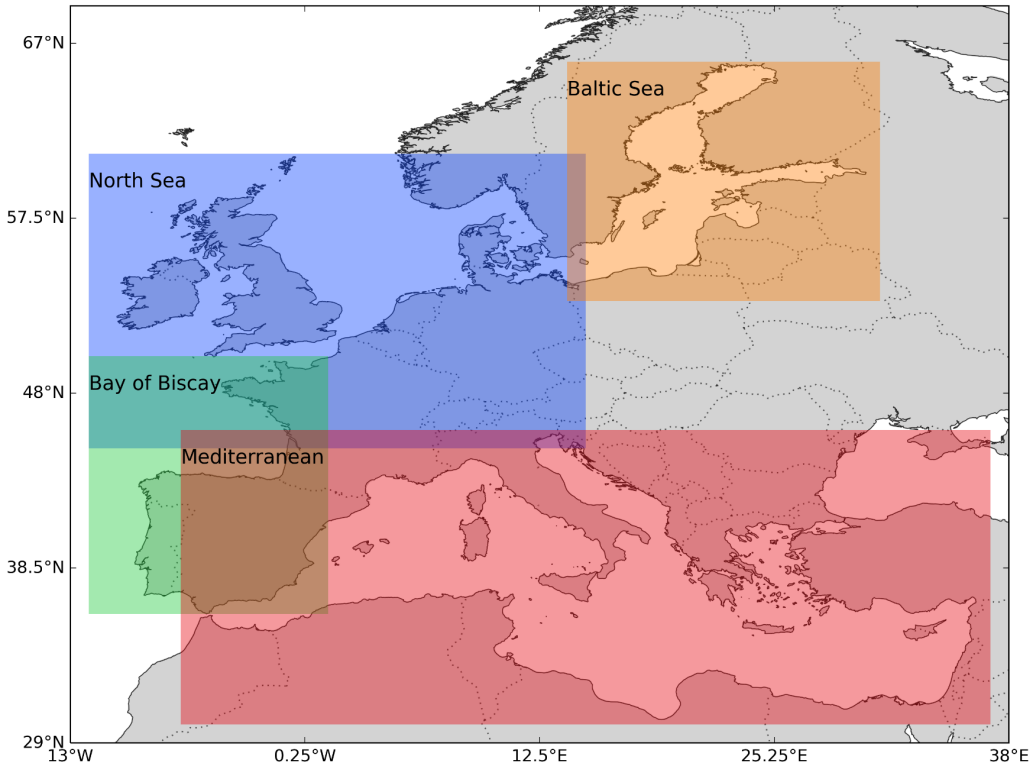

Figure 1 Map showing the 4 FutureMARES European regions for statistical downscaling of CMIP6 modelled projections; the Baltic Sea (brown), the North Sea (blue), the Bay of Biscay (green), and the Mediterranean (red).

2.3. Ensemble members and strategy of ensemble composition

We filtered models by their ability to provide a full range of variables across the historical and the three future scenarios. The CMIP6 models were accessed through the Google Cloud repository, which is not as complete as the ESGF archives, but data is more easily accessible. Compared to the datasets provided by D2.1, in the most recent version of the ensemble we selected a consolidated set of members in order to have a fixed (4-6) number of realisations per variable for a consistent representation of model spread. Still, some models are represented by several member ids (e.g., r1i1p1f1 and r3i1p1f1 for the IPSL-CM6A-LR model) or model variations (e.g., CMCC) simply because those models perform well across a range of variables. The total number of models was also kept to a lower number compared to D2.1 to reduce computational costs and time needed to repeat the model runs.

Table 1 The CMIP6 models and scenarios used for the downscaling of the various variables and scenarios.

Model name	***id***	***O_2 SSP1-2.6,SSP2-4.5, SSP5-8.5***			***Temperature SSP1-2.6,SSP2-4.5, SSP5-8.5***			***Chlorophyll SSP1-2.6,SSP2-4.5,SSP5-8.5***			***pH. SSP1-2.6,SSP2-4.5, SSP5-8.5***			***Salinity SSP1-2.6,SSP2-4.5, SSP5-8.5***		
IPSL-CM6A-LR *(Boucher et al., 2020)*	*r1i1p1f1* *r3i1p1f1*	x x	x x	x x	x x	x x	x x				x x	x x	x x	x x	x x	x x

MPI-ESM1-2-LR *(Mauritsen et al., 2019)*	*r1i1p1f1*	*x*	*x*	*x*	*x*	*x*	*x*	*x*	*x*	*x*	*x*	*x*	*x*	*x*	*x*	*x*
GFDL-ESM4 *(Dunne et al., 2020)*	*r1i1p1f1*				*x*	*x*	*x*							*x*	*x*	*x*
CMCC-ESM2 *(Lovato et al., 2022)*	*r1i1p1f1*	*x*	*x*	*x*	*x*	*x*	*x*	*x*	*x*	*x*	*x*	*x*	*x*	*x*	*x*	*x*
CMCC-CM2-SR5 *(Cherchi et al., 2019)*	*r1i1p1f1*				*x*	*x*	*x*							*x*	*x*	*x*

2.4. Scenarios

For the CM and ESM projections, expected global greenhouse gas concentrations (emerging from the Representative Concentration Pathways - RCPs) under different shared socioeconomic pathways (SSPs) up to the year 2100 (O'Neill et al., 2016) were used as external forcings. For the 6th Intergovernmental Panel on Climate Change (IPCC) report, five narratives provide alternative socio-economic developments for the world including sustainable development (SSP1), regional rivalry (SSP3), and inequality (SSP3, SSP4), fossil-fuelled development (SSP5), and middle-of-the-road development (SSP2). These are combined with green-house gas concentration trajectories that are labelled according to the radiative forcings they would approximately produce in W/m^2 by the end of this century (year 2100). While in principle the two development streams of climate scenarios and socio-economic scenarios are independent, not all combinations are feasible. This dataset, in particular, focused on the combinations SSP1-RCP2.6, SSP2-RCP4.5, and SSP5-RCP8.5, all part of the Tier1 simulations of ScenarioMIP and, therefore, were covered by a reasonable number of model realisations within CMIP6. At the same time, these combinations provided a wide spread of future scenarios corresponding roughly to strongly mitigated, middle of the road and largely unmitigated pathways. These large contrasts were needed in the FutureMARES Storylines and across all analyses in WPs 4, 5 and 6 (e.g. Global Sustainability SSP1-2.6 versus World Markets SSP5-8.5).

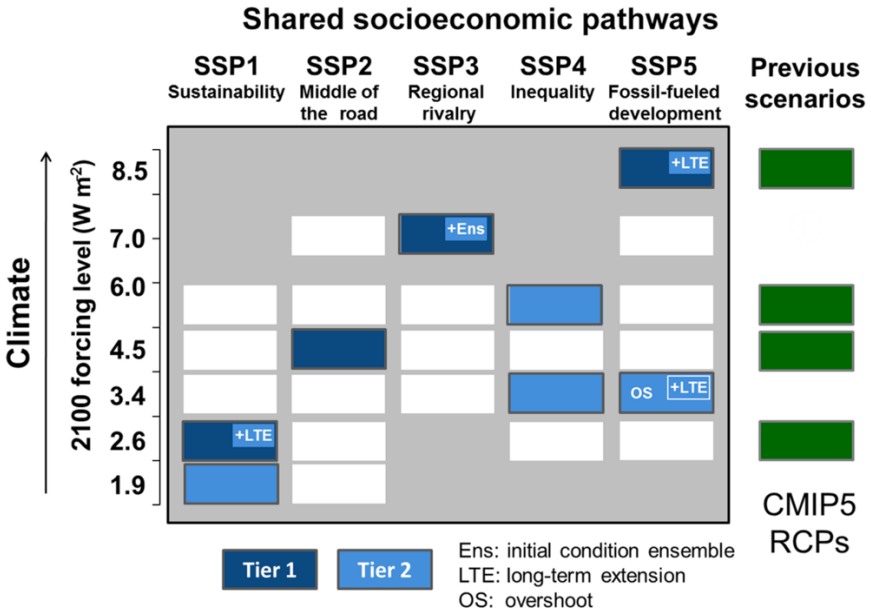

Figure 2 Overview of SSP-RCP scenarios adopted within ScenarioMIP experiments of CMIP6. (taken from O'Neill et al. 2016).

2.5. Validation of the Ensemble

In order to assess the performance of the downscaled product with respect to the original CMs and ESMs, several standard metrics were computed for the spatial fields of the seasonal climatologies of surface temperature and surface dissolved oxygen. These climatologies were compared against World Ocean Atlas climatology (Locarnini et al., 2018; Garcia et al., 2019) and then averaged over seasons. We used the recently published WOA23 for temperature and WOA18 for oxygen.

These metrics are:

- the ratio of the model mean over the mean of observations assessing the overall bias of the model fields for each season;
- the ratio of the model standard deviation over the standard deviation of observations assessing the overall spread of the model fields for each season;
- the Pearson correlation coefficient of the spatial fields from model and observations assessing the spatial mismatch of local features and local bias.

These metrics were further combined into a summary metric providing a single number for model skill. Several approaches of combinations have been used to report model skill in the literature (Nash and Sutcliffe, 1970; Gupta et al., 2009; Liu, 2020). We chose the Liu-mean efficiency skill score which provided a more balanced representation of the individual components that has shown to yield superior results to the previous methods when used in model optimisations and can, therefore, be considered more accurate (Liu, 2020).

This skill score combines the individual metrics according to the following equation:

$$LSE = 1 - \sqrt{(\rho\alpha - 1)^2 + (\beta - 1)^2},$$

where ρ is the Pearson correlation coefficient, α is the ratio of the model mean over the observation mean and β is the ration of model standard deviation over observation standard deviation.

In addition, Taylor diagrams (Taylor, 2001) were used to validate the results of the seasonal downscaled products with the CORA 5.2 (Szekely et al., 2019) dataset for global in situ temperature and salinity measurements. The skill of individual downscaled CMIP6 models is shown in these diagrams, where the seasonal cycle was removed, and we correlate timeseries (per grid point) within a single season. The figure summarizes the standard deviations of both the observations and downscaled product, the root-mean square difference (centred), and their correlations. More specifically, in each diagram, the radial axis indicates the standard deviations (the dashed circle indicates the observed one), while the seasonal correlations with observations are given by the azimuthal angle. The radial distance from the black star on the x-axis shows the unbiased root-mean square difference to the observations for individual CMIP6 models and the ensembles.

2.6. Uncertainty Assessment

The uncertainties in the downscaled ensemble product were assessed by evaluating the three principal categories of uncertainty in these types of simulations (Hawkins and Sutton, 2009):

- scenario uncertainty, the uncertainty related to the different green-house gas concentration and shared socioeconomic pathways affecting the global climate;
- model uncertainty, the uncertainty related to the different structure and parametrisation of the CMs and ESMs;
- internal variability, the uncertainty related to the natural variability of the climate system in absence of external forcing caused by intrinsic processes of the ocean, atmosphere and land dynamics.

These three components have different relative importance at different lead times of a climate projection with the latter two dominating at shorter time scales, while the scenario uncertainty becomes increasingly important as the projection evolves with time due to the increasing spread between the scenario pathways (Frölicher et al., 2016).

In our uncertainty assessment in this report, we illustrate the spatial distribution of changes in three key ecosystem pressure indicators induced by anthropogenic greenhouse gas emissions relating them to each source of uncertainty via their ratio (|change|/uncertainty). Significant changes are indicated where the ratio exceeds values of 1.

For the purpose of this assessment, future changes were computed from the ensemble mean for the middle of the road Scenario (SSP2-4.5) for the mid- and long-term IPCC assessment periods (2041-2060 and 2081-2100 respectively) by subtracting the mean conditions of the present-day time slice (1995-2014) from the mean conditions of the future time slice.

The uncertainty fields used to compute the significance ratios for each source of uncertainty were computed as follows:

- scenario uncertainty: changes were computed for each scenario in the same way as for the baseline scenario SSP2-4.5 described above. The uncertainty was then determined as the min-max range of all scenarios in each spatial pixel;

- model uncertainty: changes were computed for each individual model realisation of the baseline scenario SSP2-4.5 in the same way as for the ensemble mean described above. The uncertainty was then determined as the min-max range of all model realisations in each spatial pixel;
- the evolution of annual means in the ensemble mean of the baseline scenario projection including the historical period was detrended using a 21 year annual mean to remove long-term variability. Internal variability was then approximated by the interannual variability of this time series, i.e. the min-max range of the detrended time-series in each pixel.

The results from this assessment are provided as spatial maps of the change in each variable and its significance levels with respect to each source of uncertainty. This spatial representation allows for an appreciation of the varying importance of the sources of uncertainty at different locations.

3. Results

3.1 Validation

In the following, we compare the SD results against available observational datasets. We focused on temperature and oxygen as key indicators for the purpose of this report for which comprehensive datasets exist that allow for a spatially representative comparison. We compared the ensemble and its members against the spatially continuous WOA climatology for surface temperature and dissolved oxygen to obtain spatially continuous gapless comparison. In addition, we compared surface temperatures against the temporally comprehensive but spatially discrete in-situ data collection of the CORA5.2 dataset.

To gain an appreciation of the improvements achieved by the bias adjustment and statistical downscaling that was applied to the CMs and ESMS considered in the ensemble we compare the performance of the SD products against the performance of the original ESMs both with respect to the WOA climatologies of surface temperature and surface oxygen.

The performance of the model products was summarised by the Liu-Mean Efficiency in Figure 7 for the SD products and in Figure 8 for the original ESMs. It shows a clear improvement in model skill for both surface temperature and surface oxygen across all regions with a higher skill for temperature compared to oxygen with a difference of around 0.2 - 0.4 points. It is worth noting that the BA and SD have significantly reduced model differences in performance while for the original ESMs the inter-model differences can be substantial. The skill score also points to individual performance issues that solicitate further investigation.

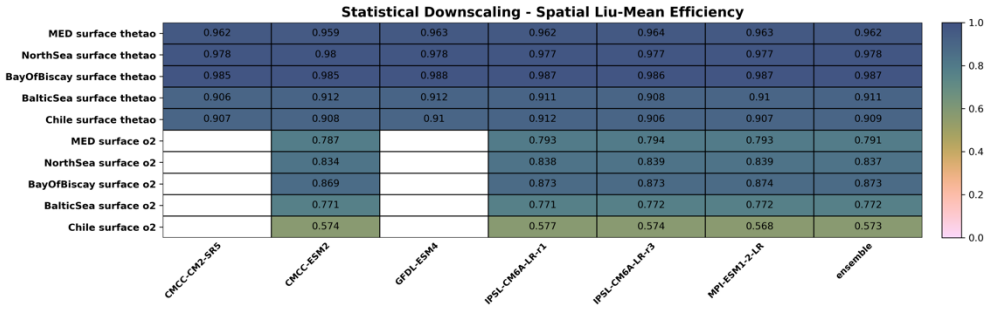

Figure 3 Liu-Mean Efficiency of the Statistical Downscaling Products for surface temperature (thetao) and surface oxygen (o2) for each basin. The evaluation is based on present day seasonal averages against WOA climatology.

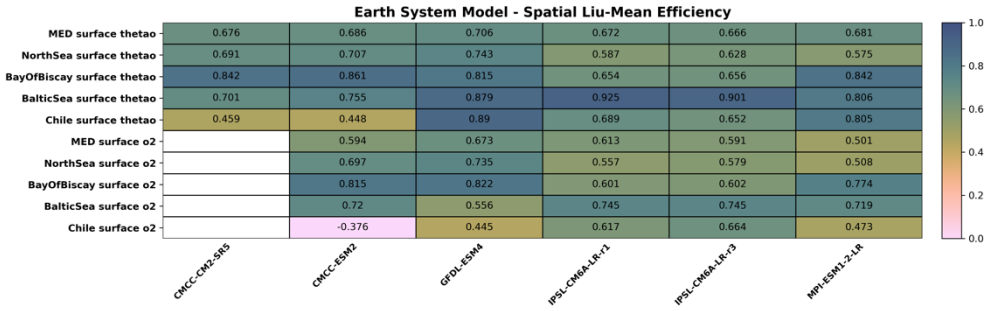

Figure 4 Liu-Mean Efficiency of the original Earth System Models for surface temperature (thetao) and surface oxygen (o2) for each basin. The evaluation is based on present day seasonal averages against WOA climatology.

The decomposition of the performance analysis into its components (Figure 9 to Figure 14) shows that, for the SD products, the penalisation of the skill score was mainly attributable to the spatial correlation coefficient (Figure 9), while the ratio of means and ratio of standard deviations were essentially flawless for these products. For the original CM and ESM simulations, the ratio of means was also generally very close to 1, but both the Pearson correlation and the ratio of standard deviation indicate substantial shortcomings in skill. However, as for SD products the main driver for lack of skill was also a deficiency in correlation which is significantly stronger than the mismatches of standard deviations.

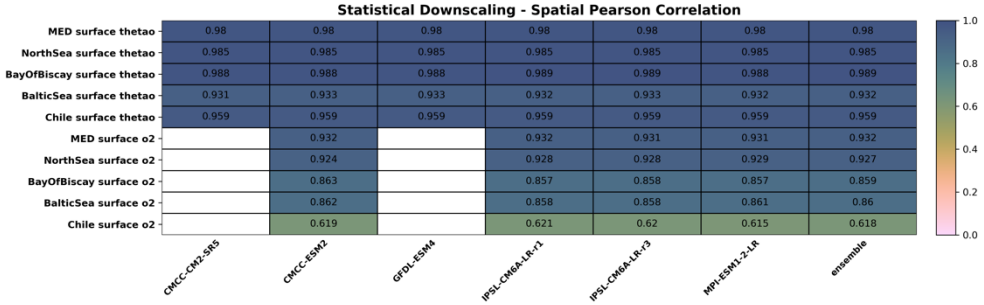

Figure 5 Pearson Correlation for the Statistical Downscaling Products for surface temperature (thetao) and surface oxygen (o2) for each basin. The evaluation is based on present day seasonal averages against WOA climatology.

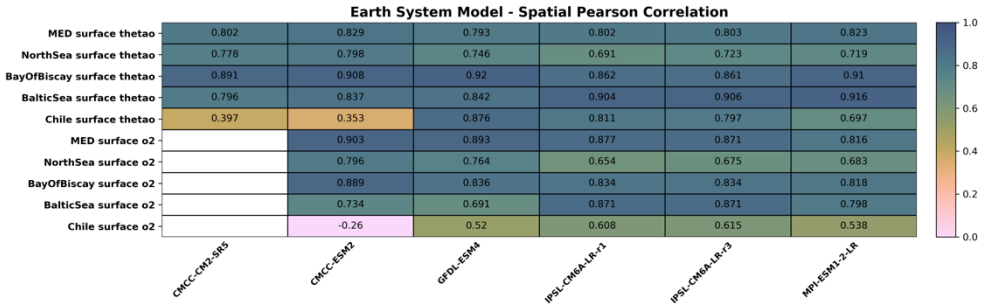

Figure 6 Pearson Correlation for the original Earth System Models for surface temperature (thetao) and surface oxygen (o2) for each basin. The evaluation is based on present day seasonal averages against WOA climatology.

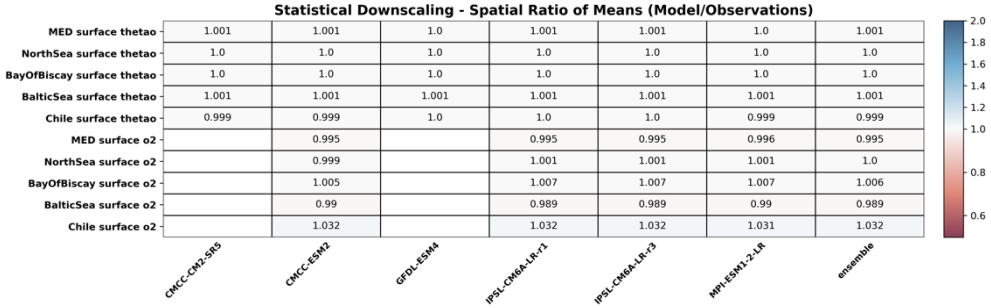

Figure 7 Ratio of Means for the Statistical Downscaling Products for surface temperature (thetao) and surface oxygen (o2) for each basin. The evaluation is based on present day seasonal averages against WOA climatology.

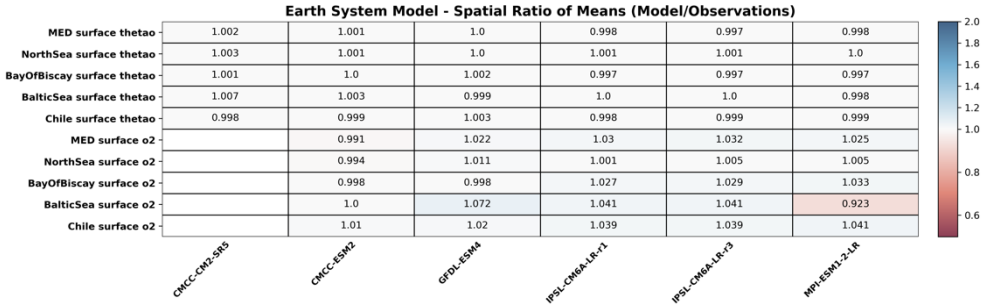

Figure 8 Ratio of Means for the original Earth System Models for surface temperature (thetao) and surface oxygen (o2) for each basin. The evaluation is based on present day seasonal averages against WOA climatology.

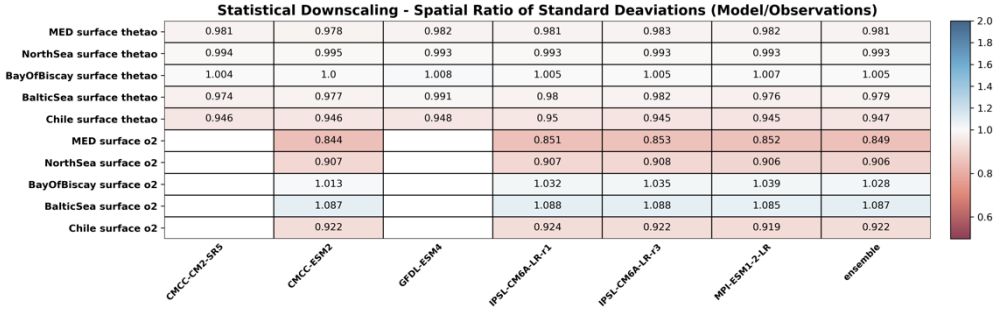

Figure 9 Ratio of Standard Deviations for the Statistical Downscaling Products for surface temperature (thetao) and surface oxygen (o2) for each basin. The evaluation is based on present day seasonal averages against WOA climatology.

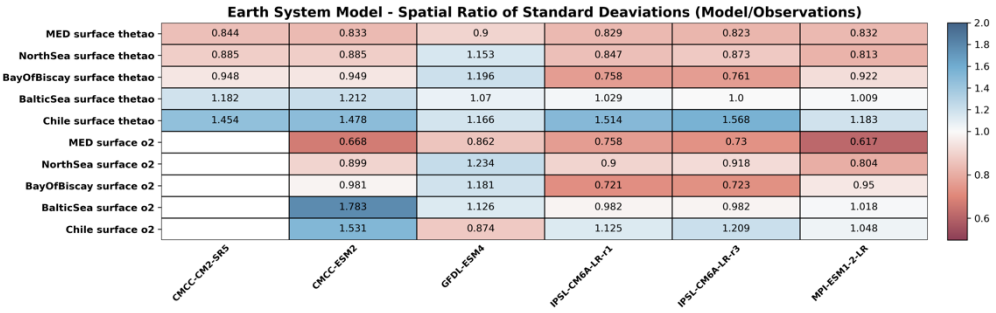

Figure 10 Ratio of Standard Deviations for the original Earth System Models for surface temperature (thetao) and surface oxygen (o2) for each basin. The evaluation is based on present day seasonal averages against WOA climatology.

Figure 3 to Figure 6 show the Taylor diagrams for the comparison of the surface temperatures in the ensemble average against the CORA 5.2 dataset. The variability across the ensemble compared very well to the variability in the observations except for the Baltic Sea. In the Baltic Sea, variability differences between models and observations were slightly higher compared to the other regions with overestimation by the models in winter and spring and underestimation in summer and autumn.

Correlations between model and observations were generally high, around 0.9 or higher, with the lowest correlation for all regions (around 0.8) occurring in winter and in the Baltic Sea as low as 0.7.

Similarly, root mean-square differences were highest in winter but remained mostly at values around 1 or lower.

Skill differences between model realisations were comparatively low with none of the ensemble members being particularly high or low in skill compared to the others. The highest spread (differences) between models occurred for the Winter season in the Baltic Sea.

Overall, the SD products compared well against the CORA 5.2 dataset, particularly considering that these are based on uninitialised CM or ESM simulations that, by design, cannot capture the phase of the short-term variability.

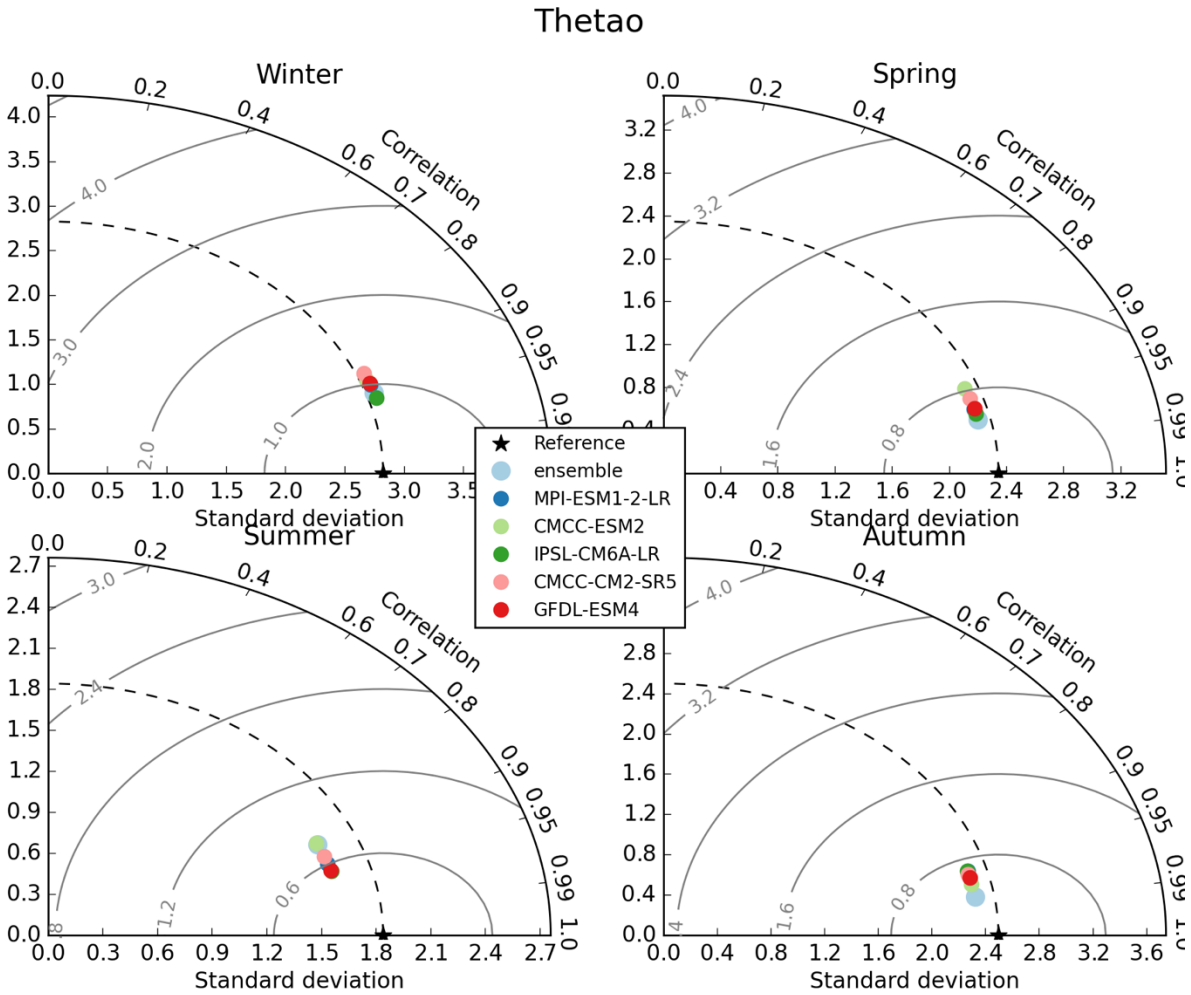

Figure 11 Taylor diagram for the temperature at 5 m depth compared with CORA 5.2 for the Mediterranean.

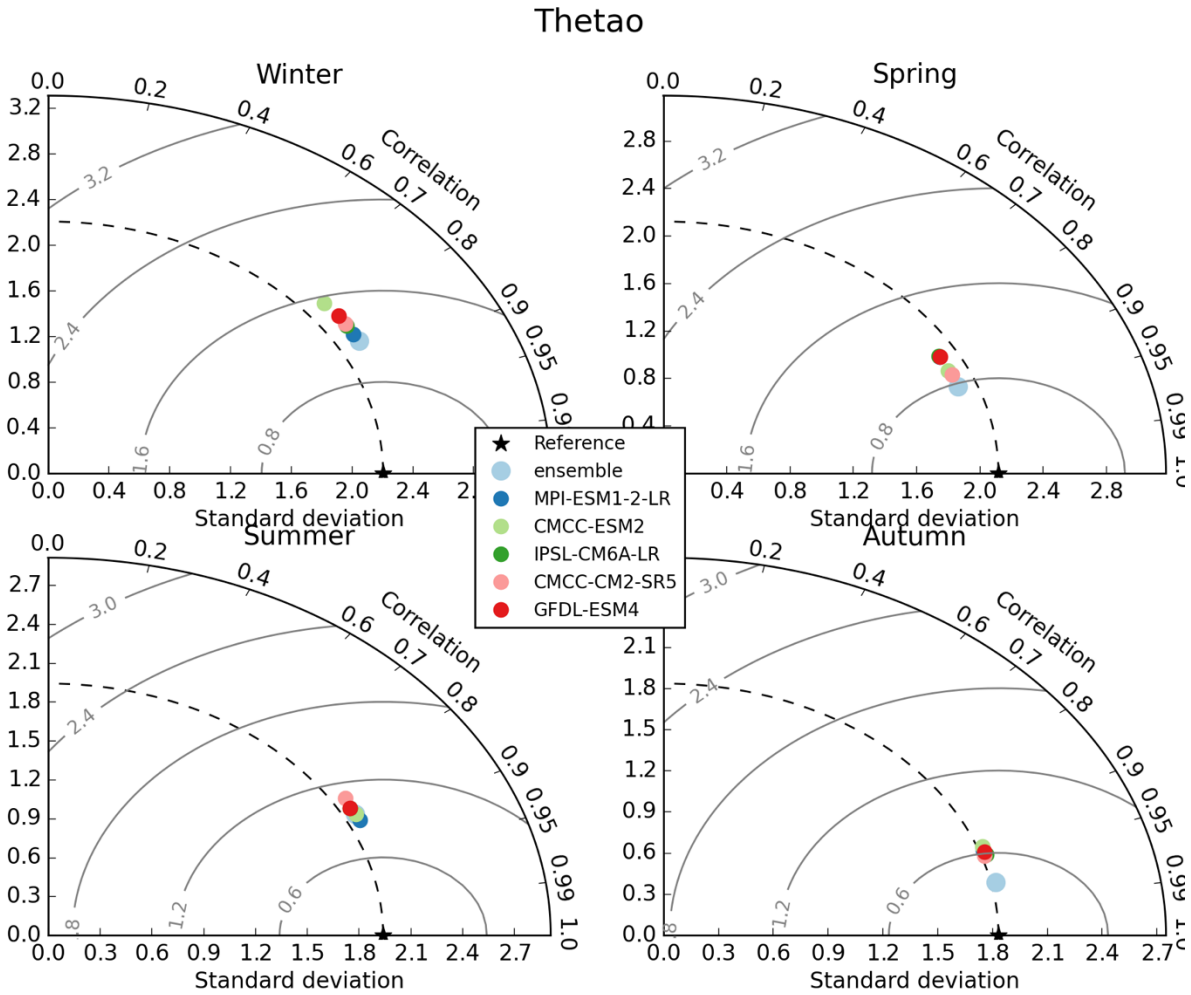

Figure 12 Taylor diagram for the temperature at 5 m depth compared with CORA 5.2 for the North Sea.

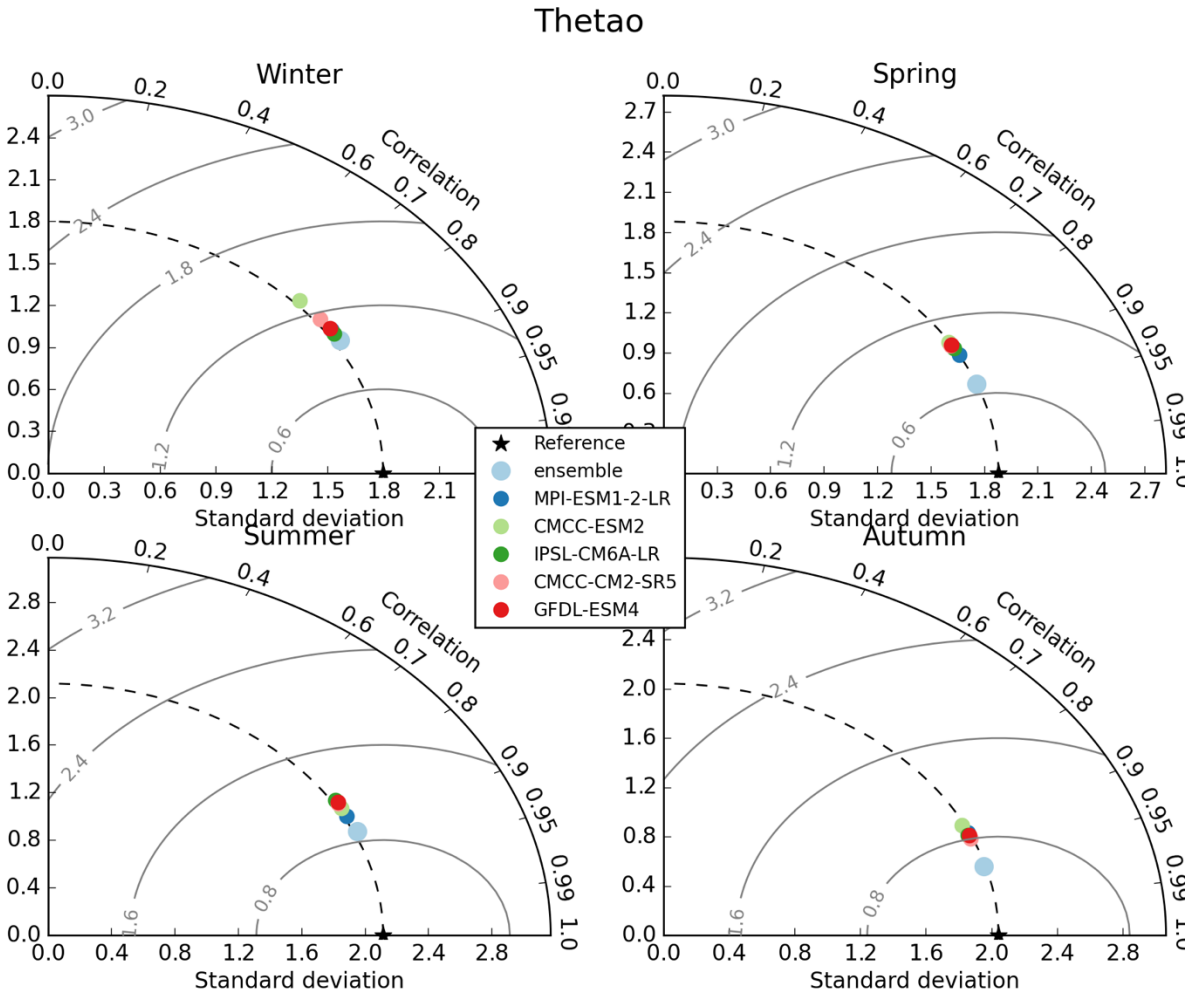

Figure 13 Taylor diagram for the temperature at 5 m depth compared with CORA 5.2 for the Bay of Biscay.

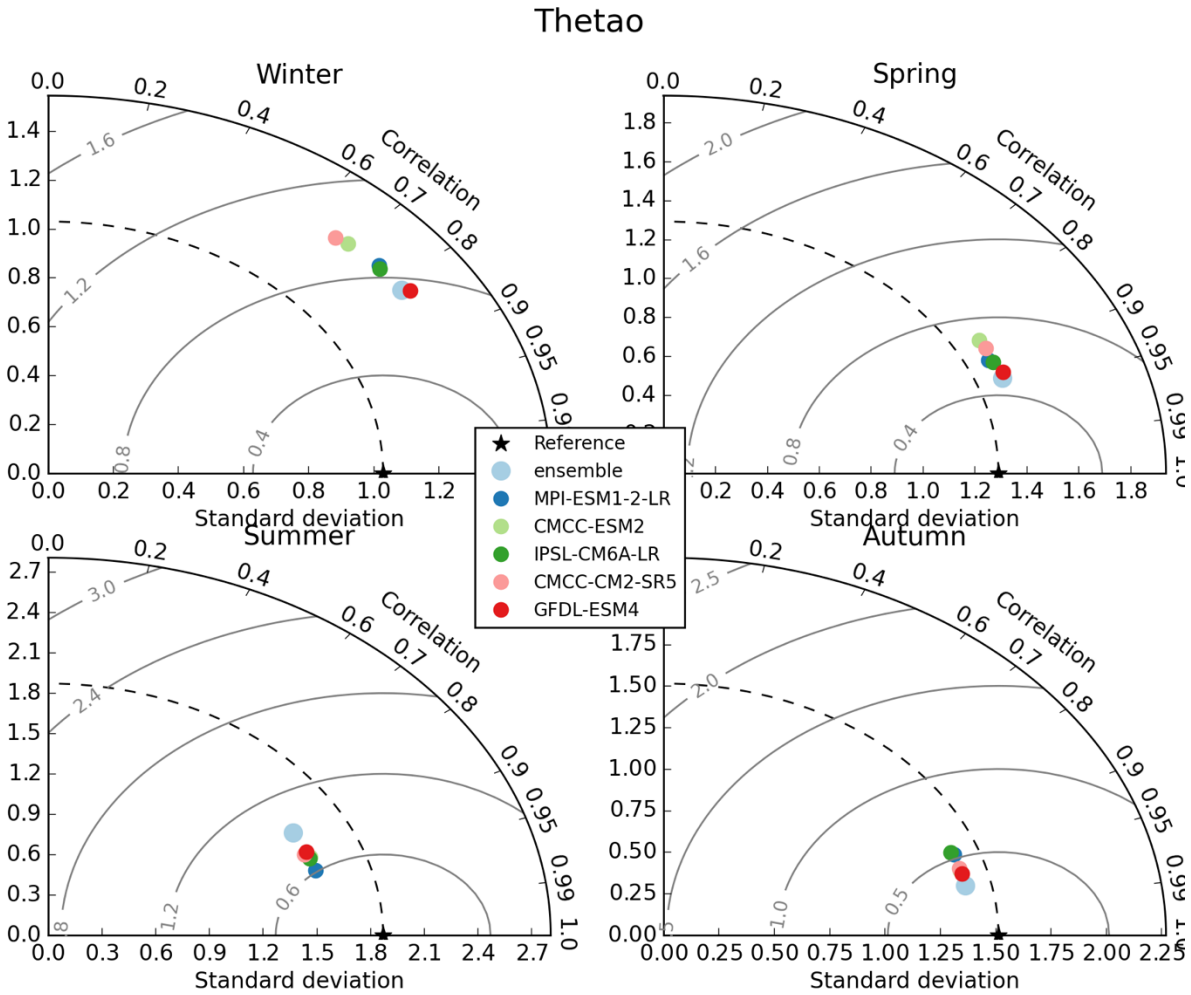

Figure 14 Taylor diagram for the temperature at 5 m depth compared with CORA 5.2 for the Baltic Sea.

3.2 Uncertainty across Regions

In this section, we illustrate the changes induced by anthropogenic greenhouse gas emissions in three key ecosystem pressures: two direct pressures, warming (represented by the sea surface temperature) and acidification (represented by surface pH) and one indirect pressure, deoxygenation (represented by bottom dissolved oxygen). The latter is considered to be an indirect pressure here as it is a cumulative result of the other pressures and their effect on the ocean dynamics and the biological production in the water column. The significance of the induced changes was further analysed by comparing them to three separate sources of uncertainties in climate projections: i) internal variability, ii) model uncertainty, and iii) scenario uncertainty. In the following subsections, we present the results of this analysis by region.

3.2.2 Mediterranean Sea

Figure 15 shows the Mediterranean Sea basin average timeseries of the three ecosystem pressure indicators from the recent past up to the end of this century for the three different scenarios represented by the SD ensemble product. The patterns are qualitatively comparable to those observed for the global mean trajectories (IPCC, 2021; Kwiatkowski et al., 2020). For the unmitigated scenario SSP5-8.5 (FutureMARES World Markets) the bulk surface temperature of the Mediterranean Sea rises gradually up to 5 °C higher than present day. For the middle of the road scenario SSP2-4.5, the increase in temperature from present day is substantially lower reaching approximately 2 °C. For the strongly mitigated scenario SSP1-2.6 (FutureMARES Global Sustainability), the temperature initially increases then stabilizes towards the middle of the century at around 1.5 °C of warming. Model spread is moderately high (2.5 to 3.0 °C), such that the differences between the two scenarios producing weaker warming are partially blurred, while for the strong warming the difference in temperature emerges from the model uncertainty. Interannual variability is low compared to the long-term changes. In terms of ocean acidification, SSP5-8.5 shows a strong gradual decrease in ocean pH up to about 0.4 units from present day conditions, while SSP2-4.5 stabilizes towards the end of the century at about a 0.2 decrease in pH. SSP1-2.6 shows a slightly reversing trend, limiting the overall decrease in pH to less than 0.1 units in 2100. Uncertainty for this variable is inherently low and differences in the changes are clear. For bottom oxygen, uncertainty was highest relative to the changes observed among the three scenarios. For all three scenarios, oxygen decreases, by 0.5 ml/l for SSP5-8.5, and approximately 0.2 for SSP2-4.5 and 0.1 for SSP1-2.6.

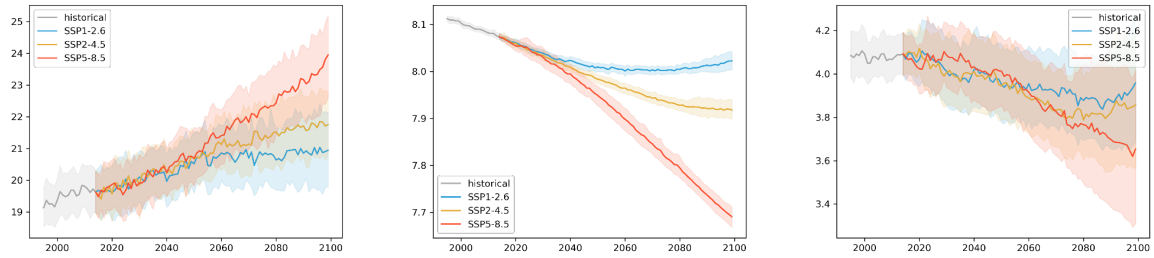

Figure 15 Time series of Mediterranean Sea average surface temperature (°C), pH and bottom oxygen [ml/l] over the historical time slice and the three scenarios. Full lines show the ensemble, shaded areas show the ensemble spread based on the 2.5 and 97.5 percentiles of the model distributions.

To give a clearer picture of the relative importance of the different sources of uncertainty and their role in different locations, Figure 16 and Figure 17 show maps of the changes of the three indicators for the ensemble average of scenario SSP2-4.5 as absolute values and relative to the uncertainties in each spatial point. It can be seen that surface temperature rise is strongest in the Adriatic and Aegean Sea with generally higher changes in the Eastern compared to the Western Basin. Warming almost doubles from mid to the end of the century with no major difference in the spatial distribution of changes in between the two time slices. At mid-century interannual variability and model uncertainty are of the order of the changes across the basin while the differences in between the scenarios are significantly lower than the changes induced. This situation essentially inverts for the long-term changes which become a little more significant with respect to interannual variability, while the difference between the scenarios have grown relatively to be comparable to the magnitude of change.

Acidification in the Mediterranean results strongest in the Northern Adriatic with generally slightly higher decreases of pH in the Northern parts compared to the Southern coast of the basin. As could be inferred from the basin mean time series, changes are strongly significant for both time slices with respect to interannual variability and model uncertainty, while the

difference in between the mitigation pathways are of the order of the changes at mid-century and dominate the signal towards the end of the century.

For bottom dissolved oxygen the situation is much less clear. While on average a decrease in seafloor oxygen is visible from the time series, some areas even show increase in oxygen for the ensemble mean (most evident in the Aegean Sea), interannual variability and particularly model uncertainty is high in these areas. Areas of oxygen decrease on the contrary clearly emerge from interannual variability and are also slightly significant with respect to model uncertainty. Similarly changes in mitigation pathways play a much more important role in areas of oxygen increase with respect to the areas of decrease, where the differences between scenarios are smaller than the induced decrease.

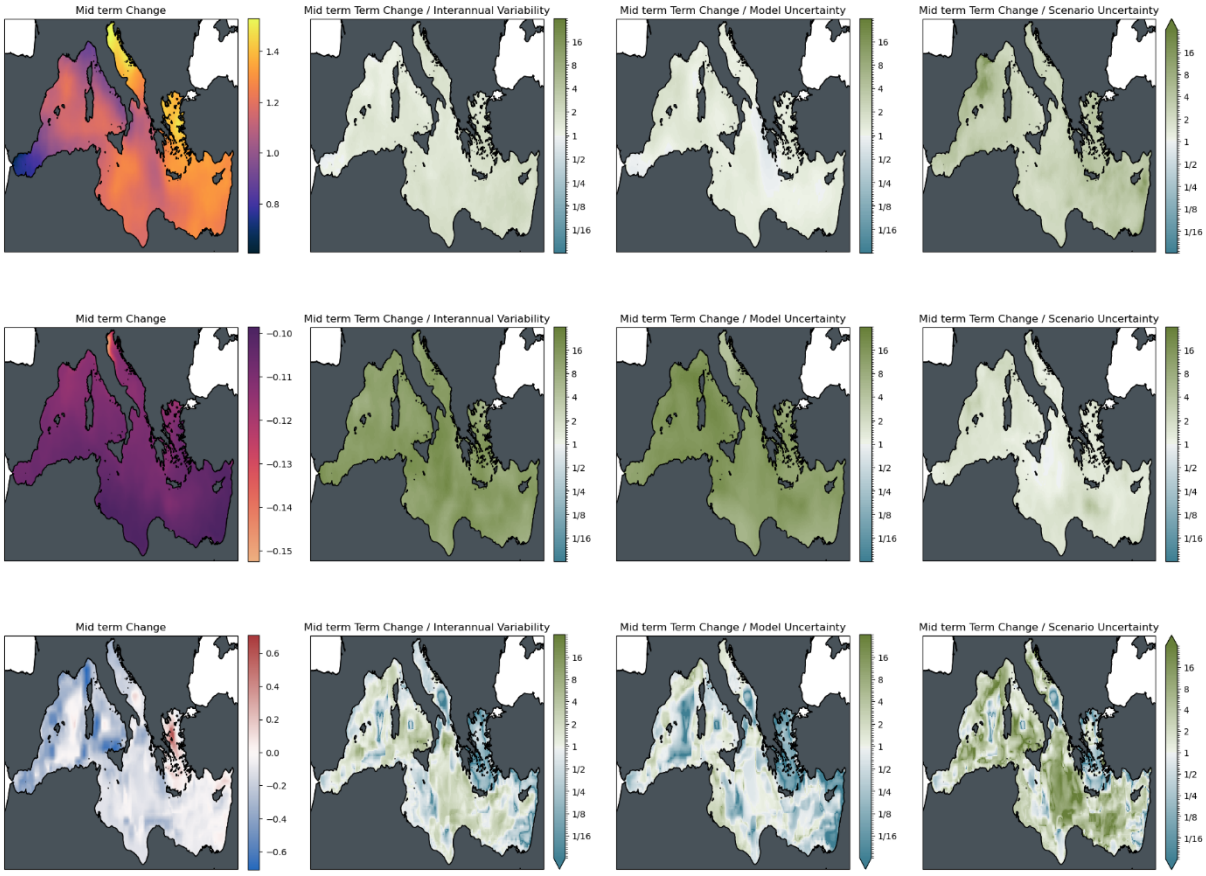

Figure 16 Significance of mid-term changes in the Mediterranean Sea against three sources of uncertainty under scenario SSP2-4.5 for three ecosystem pressures. From left to right: changes between long-term conditions (2081-2100 mean) and present-day conditions (1995-2014); changes relative to internal variability; changes relative to model uncertainty; changes relative to scenario uncertainty. Top to bottom: Surface Temperature [K]; surface pH; bottom dissolved oxygen [ml/l].

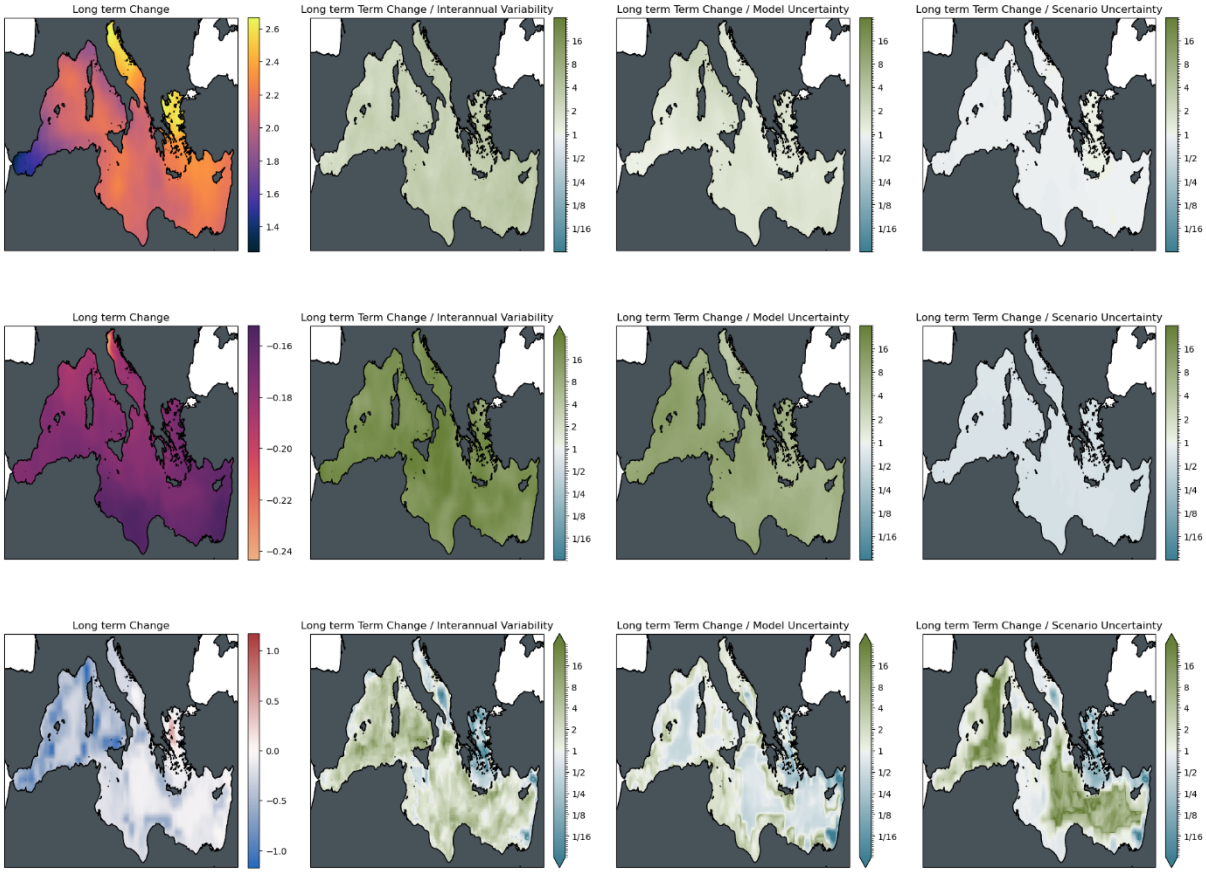

Figure 17 Significance of long-term changes in the Mediterranean Sea against three sources of uncertainty under scenario SSP2-4.5 for three ecosystem pressures. From left to right: changes between long-term conditions (2081-2100 mean) and present-day conditions (1995-2014); changes relative to internal variability; changes relative to model uncertainty; changes relative to scenario uncertainty. Top to bottom: Surface Temperature [K]; surface pH; bottom dissolved oxygen [ml/l].

3.2.1 North Sea

The basin-scale mean evolution of induced changes in the wider North Sea area (Figure 18) was similar to the changes in the Mediterranean Sea. Warming is a less accentuated though with only three degrees increase at the end of the century for the unmitigated scenario SSP5-8.5 and less than a degree for the moderate and strong mitigation scenarios. Acidication levels range from little less than 0.1 units (SSP1-2.6) to around 0.5 units of decrease in surface pH (SPP5-8.5), while seafloor oxygen decrease (~0.1 – 0.3 ml/l) is a little less evident due to a higher internal variability (up to ~0.2 ml/l) `compared to the that observed in the Mediterranean Sea.

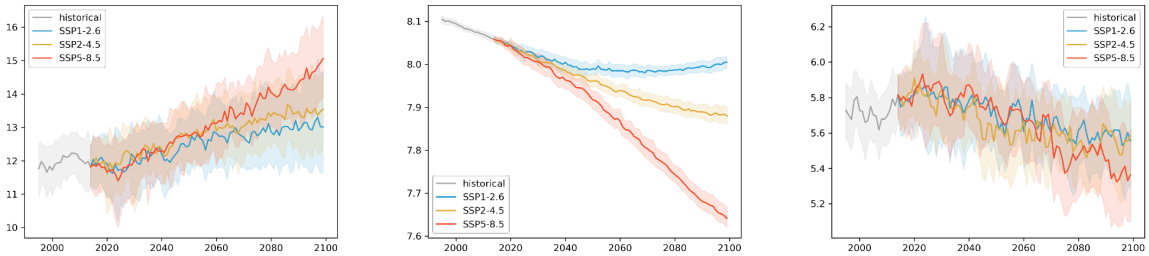

Figure 18 Time series of North Sea average surface temperature (°C), pH and bottom oxygen [ml/l] over the historical time slice and the three scenarios. Full lines show the ensemble, shaded areas show the ensemble spread based on the 2.5 and 97.5 percentiles of the model distributions.

Looking in more detail at the spatial distribution of changes and uncertainties (Figure 19 and Figure 20) it can be observed that warming is strongest towards the Eastern parts of the European shelf, while comparatively week towards the open Atlantic. These trends however are only very weakly emerging with respect to internal variability and model uncertainty on most of the continental shelf while they are generally slightly overshadowed by internal variability and model uncertainty in the oceanic parts (except for the long-term changes with respect to interannual variability that are slightly emerging throughout the domain). The difference between the mitigation pathways is only of minor importance at mid-century (approximately 1/3 of the change signal across the basin) but reaches about the same order of magnitude as the induced change in the long-term. Seafloor oxygen changes in the ensemble average are of considerable magnitude only in the open ocean areas along the shelf break where dissolved oxygen is declining by up to 1 ml/l. These changes are only mildly emerging at mid-century while they become increasingly significant towards the end of the century. The difference of these changes between mitigation scenarios is minor even towards the end of the century.

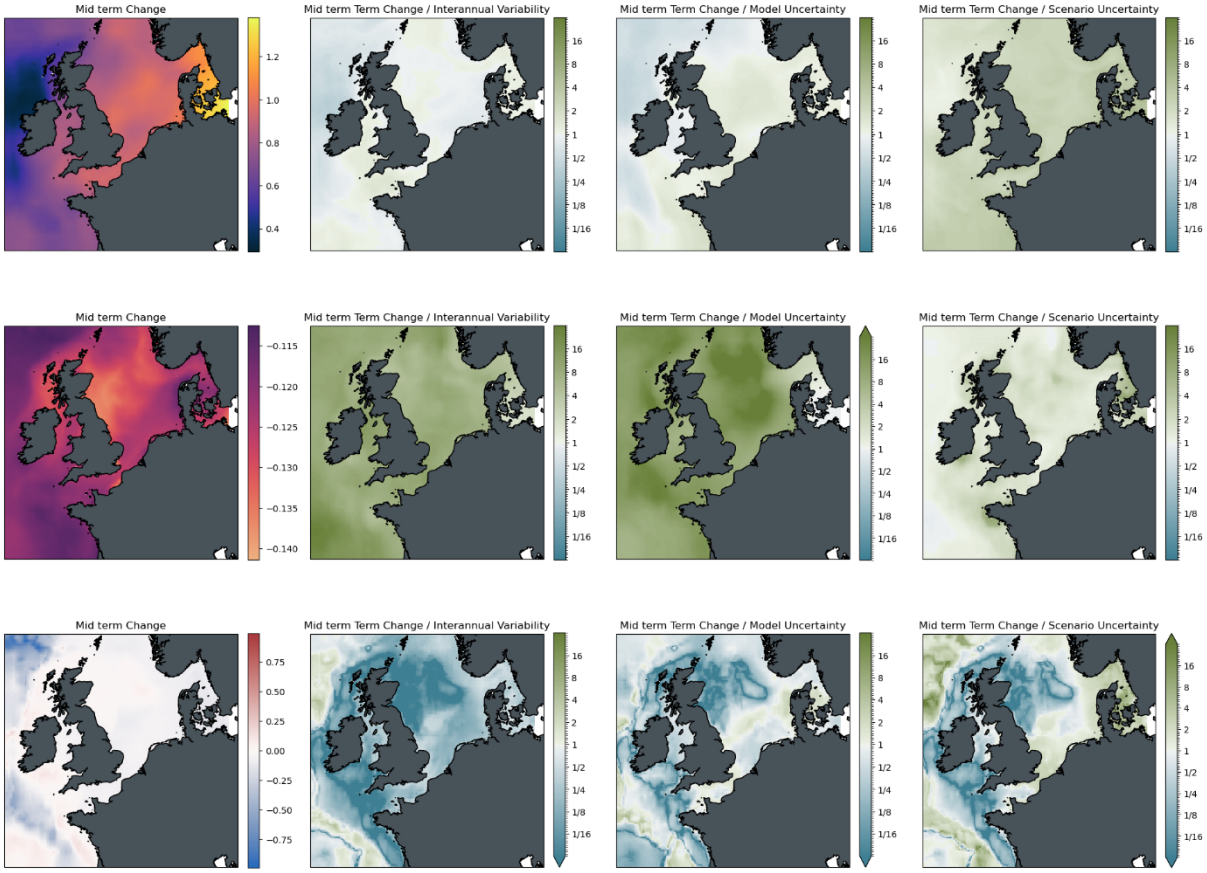

Figure 19 Significance of mid-term changes in the North Sea against three sources of uncertainty under scenario SSP2-4.5 for three ecosystem pressures. From left to right: changes between long-term conditions (2081-2100 mean) and present-day conditions (1995-2014); changes relative to internal variability; changes relative to model uncertainty; changes relative to scenario uncertainty. Top to bottom: Surface Temperature [K]; surface pH; bottom dissolved oxygen [ml/l].

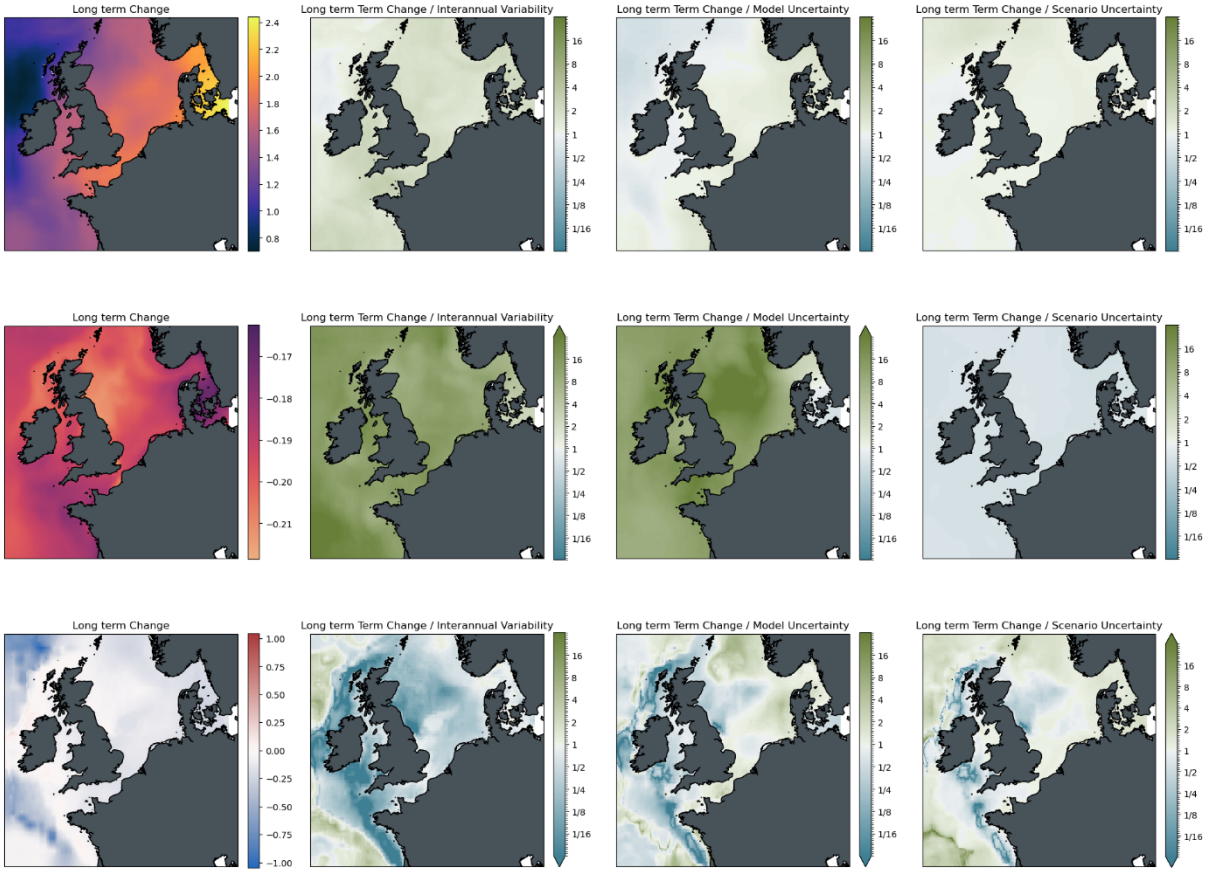

Figure 20 Significance of long-term changes in the North Sea against three sources of uncertainty under scenario SSP2-4.5 for three ecosystem pressures. From left to right: changes between long-term conditions (2081-2100 mean) and present-day conditions (1995-2014); changes relative to internal variability; changes relative to model uncertainty; changes relative to scenario uncertainty. Top to bottom: Surface Temperature [K]; surface pH; bottom dissolved oxygen [ml/l].

3.2.3 Bay of Biscay

In the area around the Bay of Biscay the domain averages roughly follow the pattern of the previous two regions with strong continuous warming up to 3 degrees by 2100 and acidification of up to 0.4 pH units for SSP5-8.5 and gradually attenuated trends for the moderate to strong mitigation scenarios (with pH starting to revert the acidification trend in the second half of the century for SSP1-2.6). Acidification trends are strongly significant while the warming trends emerge less clearly due to considerable model uncertainty (~1.5 up to 3.5 degrees), particularly for the two pathways producing weaker changes. Deoxygenation shows considerable model (~0.4-0.5 ml/l) and interannual variability (up to 0.2 ml/l). Curiously, trends appear almost absent for the strongest scenario for the first couple of decades, followed by a few years of strong interannual variability and a rapid decay in surface oxygen that then continues more gradually until the end of this century, while the other two scenarios show a weaker, more continuous decay similar to the other two regions illustrated above.

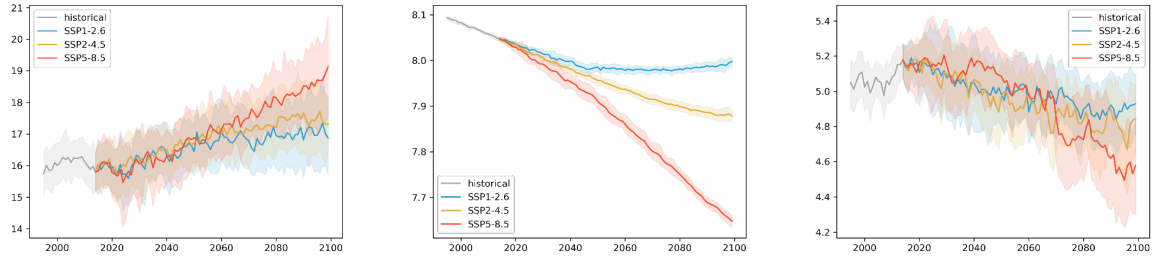

Figure 21 Time series of Bay of Biscay average surface temperature (°C), pH and bottom oxygen [ml/l] over the historical time slice and the three scenarios. Full lines show the ensemble, shaded areas show the ensemble spread based on the 2.5 and 97.5 percentiles of the model distributions.

The spatial distribution of these domain average patterns (Figure 22 and Figure 23) indicates the Northern coast of the Iberian Peninsula and the northern coast of Britany as focal points of surface warming with the former one particularly strong in the mid-term (up to 1 degree) and the latter particularly strong in the long-term (almost 2 degrees). Relative to interannual variability and model uncertainty however these changes are only slightly emerging in the mid-term, while changes in the deeper Atlantic are subject to significant ranges of uncertainty for these two sources. In the long-term changes become significant with respect to interannual variability while model uncertainty remains present to the same degree as in the mid-term. As for the previous domains, warming is only mildly affected by the differences of mitigation pathways in the mid-term, while in the long-term the different mitigation strategies lead to differences in warming of the same order as the change signal itself. Acidification trends are comparatively homogeneous across the basin with little stronger trends in the off-shelf areas of the North-Eastern Atlantic. This pattern is consistent between the two time slices, however with acidification levels about 50% higher at the end of the century compared to the mid-term changes. The trends are strongly significant with respect to model uncertainty and interannual variability for both time slices. The difference between scenarios is roughly of the same order of magnitude as the induced changes at mid-century, while at the end of the century the mitigation pathways become increasingly important as the difference between scenarios reaches twice the magnitude of the change signal.

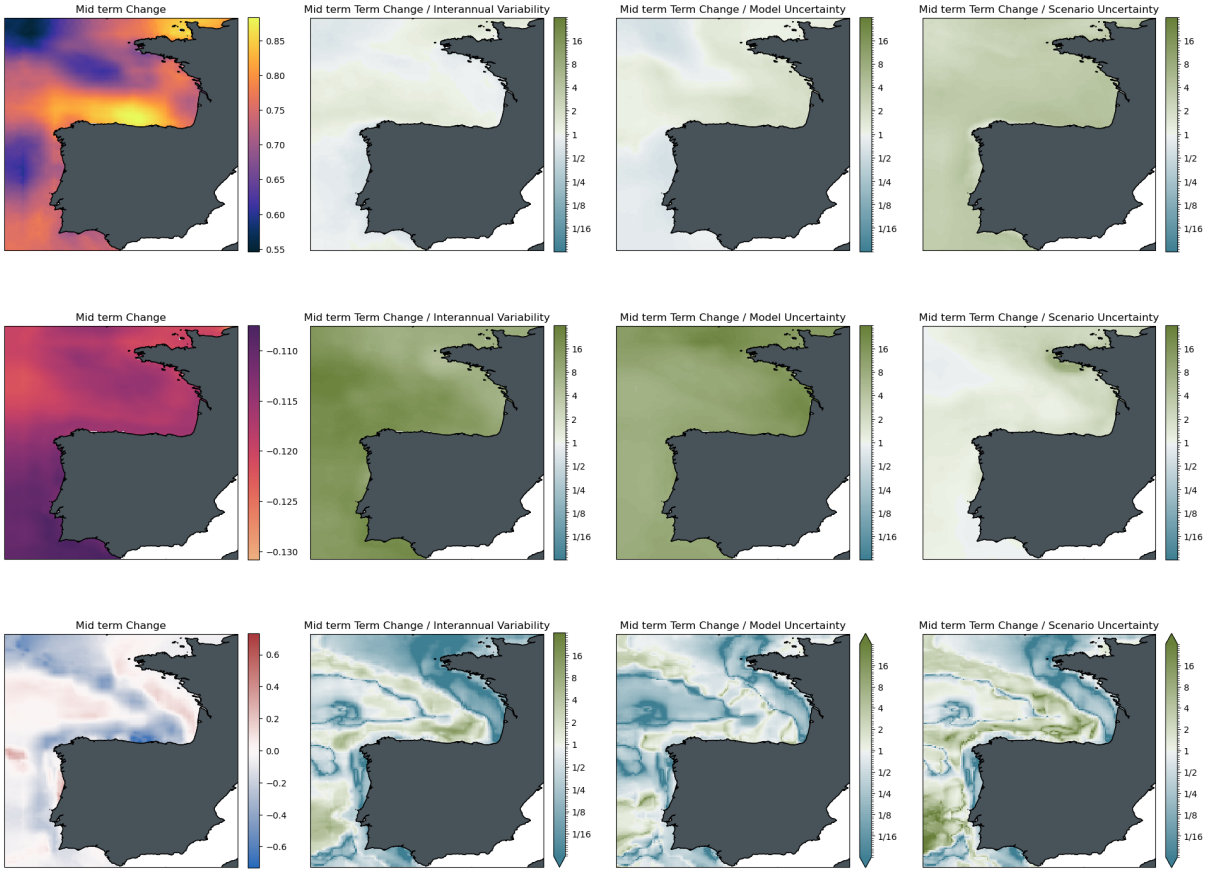

Figure 22 Significance of mid-term changes in the Bay of Biscay against three sources of uncertainty under scenario SSP2-4.5 for three ecosystem pressures. From left to right: changes between long-term conditions (2081-2100 mean) and present-day conditions (1995-2014); changes relative to internal variability; changes relative to model uncertainty; changes relative to scenario uncertainty. Top to bottom: Surface Temperature [K]; surface pH; bottom dissolved oxygen [ml/l].

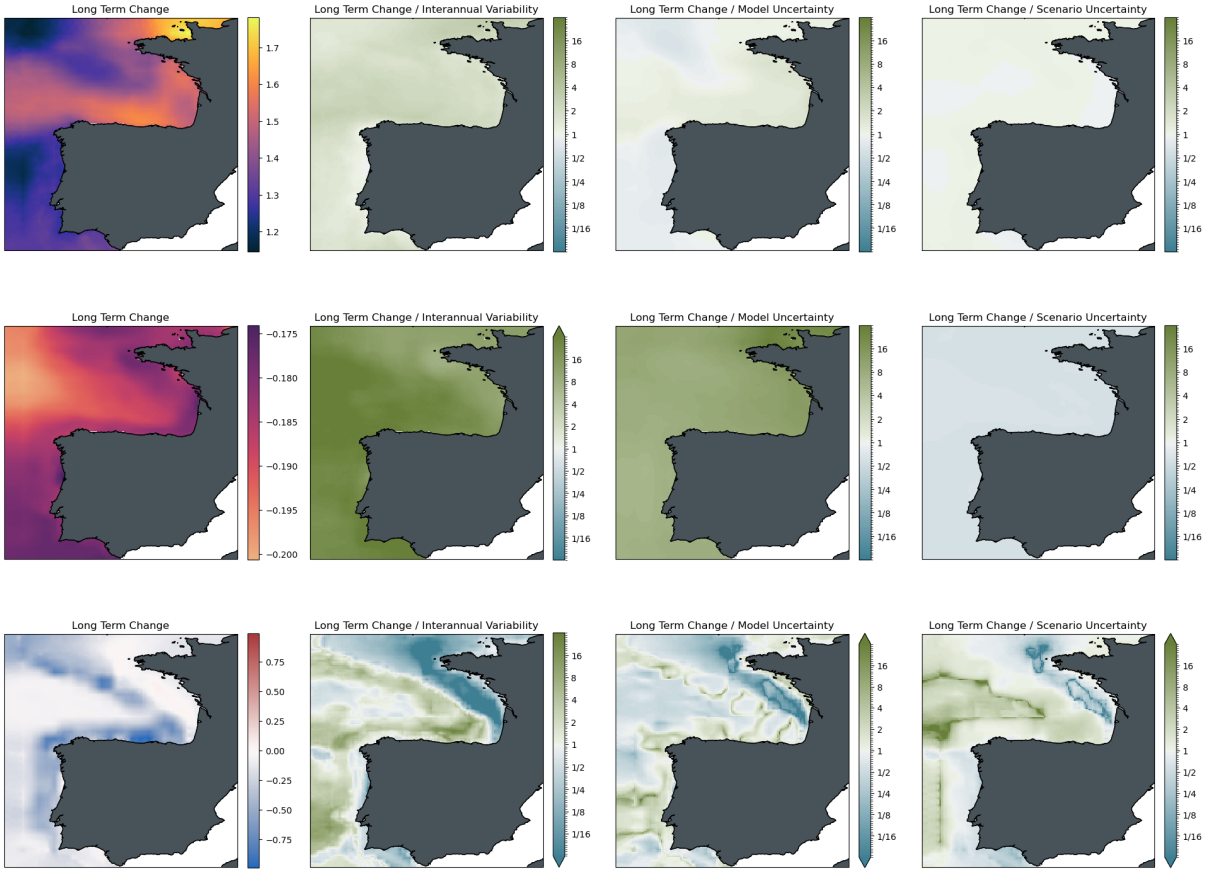

Figure 23 Significance of long-term changes in the Bay of Biscay against three sources of uncertainty under scenario SSP2-4.5 for three ecosystem pressures. From left to right: changes between long-term conditions (2081-2100 mean) and present-day conditions (1995-2014); changes relative to internal variability; changes relative to model uncertainty; changes relative to scenario uncertainty. Top to bottom: Surface Temperature [K]; surface pH; bottom dissolved oxygen [ml/l].

3.2.4 Baltic Sea

While the basin mean trends of warming, acidification and deoxygenation are present also in the Baltic Sea, their behaviour and relation to uncertainty is in some aspects substantially different in this coastal, semi-enclosed basin when compared to the other regions as shown in Figure 24. A fundamental difference is the large model uncertainty (up to 0.8 pH units) and increased interannual variability (up to 0.05 units) of surface pH with respect to the induced changes (0.1–0.5 pH units). This difference can be attributed to the fundamentally different character of this brackish water basin where pH conditions are not only driven by atmospheric carbon dioxide concentrations, but also affected by a series of coastal processes, such as changes in water catchment, precipitation patterns, weathering and liming (Gustafsson and Gustafsson, 2020). In addition, the deoxygenation trend (~0.2 ml/l) here is significantly weaker and interannual variability is significantly higher (up to 0.5 ml/l) as the oxygenation of the Baltic Sea is to a much lesser degree influenced by large scale ventilation and much more affected by coastal influences. Warming trends (2-5 degrees) on the contrary are comparatively similar to the other basins.

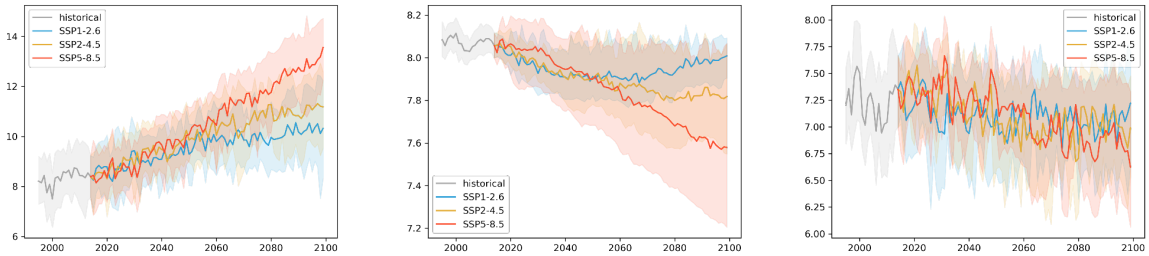

Figure 24 Time series of Baltic Sea average surface temperature (C), pH and bottom oxygen [ml/l] over the historical time slice and the three scenarios. Full lines show the ensemble, shaded areas show the ensemble spread based on the 2.5 and 97.5 percentiles of the model distribution.

Looking at regional differences in these trends (Figure 22 and Figure 23) warming in the ensemble average of the Baltic Sea for scenario SSP2-4.5 at mid century is strongest in the Bothnian Sea and the Gulf of Riga and weakest at the margins of the Bothnian Bay and the Southern Baltic Proper. This pattern persists also at the end of the century with the two warming hot-spots spreading into the Northern Baltic Proper. Compared to interannual variability and model uncertainty the trends are only weakly emerging across the basin. Differences between mitigation pathways are neglectable at mid-century but reach the order of magnitude of the induced changes by 2100. For acidification, which is strongest in the Bothnian Bay, there is a clear distinction in the impact of interannual variability and model uncertainty on the significance of the mid- and long-term trend. While trends clearly emerge from interannual variability, they are subject to significant model uncertainty as was visible already in the basin average time series that reaches more than twice the level of the trend.

The bottom oxygen field for mid-century shows deoxygenation across the whole basin except for a small cell of oxygen increase north of Gotland that extends to the whole Gotland basin at the end of the century. It should be noted however that these changes are comparatively uncertain with respect to interannual variability and model uncertainty across the entire Baltic Sea and are particularly uncertain in the area of oxygen increase. This area is also the only area in which scenario differences in oxygen trends are significantly bigger than the actual oxygen trend making it essentially an area of uncertain outcome in all aspects. In other areas, the impacts of different mitigation pathways reaches the levels of the induced changes by the end of the century.

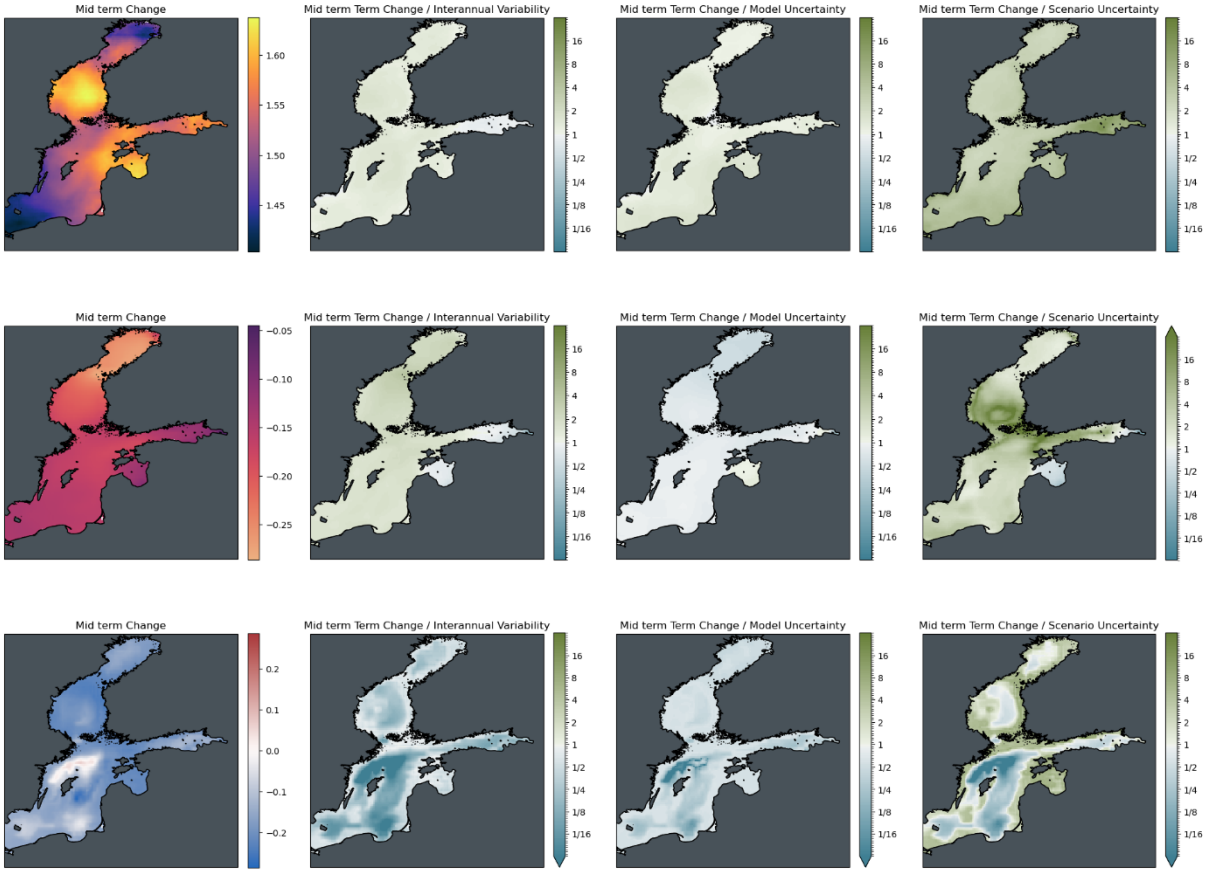

Figure 25 Significance of mid-term changes in the Baltic Sea against three sources of uncertainty under scenario SSP2-4.5 for three ecosystem pressures. From left to right: changes between long-term conditions (2081-2100 mean) and present-day conditions (1995-2014); changes relative to internal variability; changes relative to model uncertainty; changes relative to scenario uncertainty. Top to bottom: Surface Temperature [K]; surface pH; bottom dissolved oxygen [ml/l].

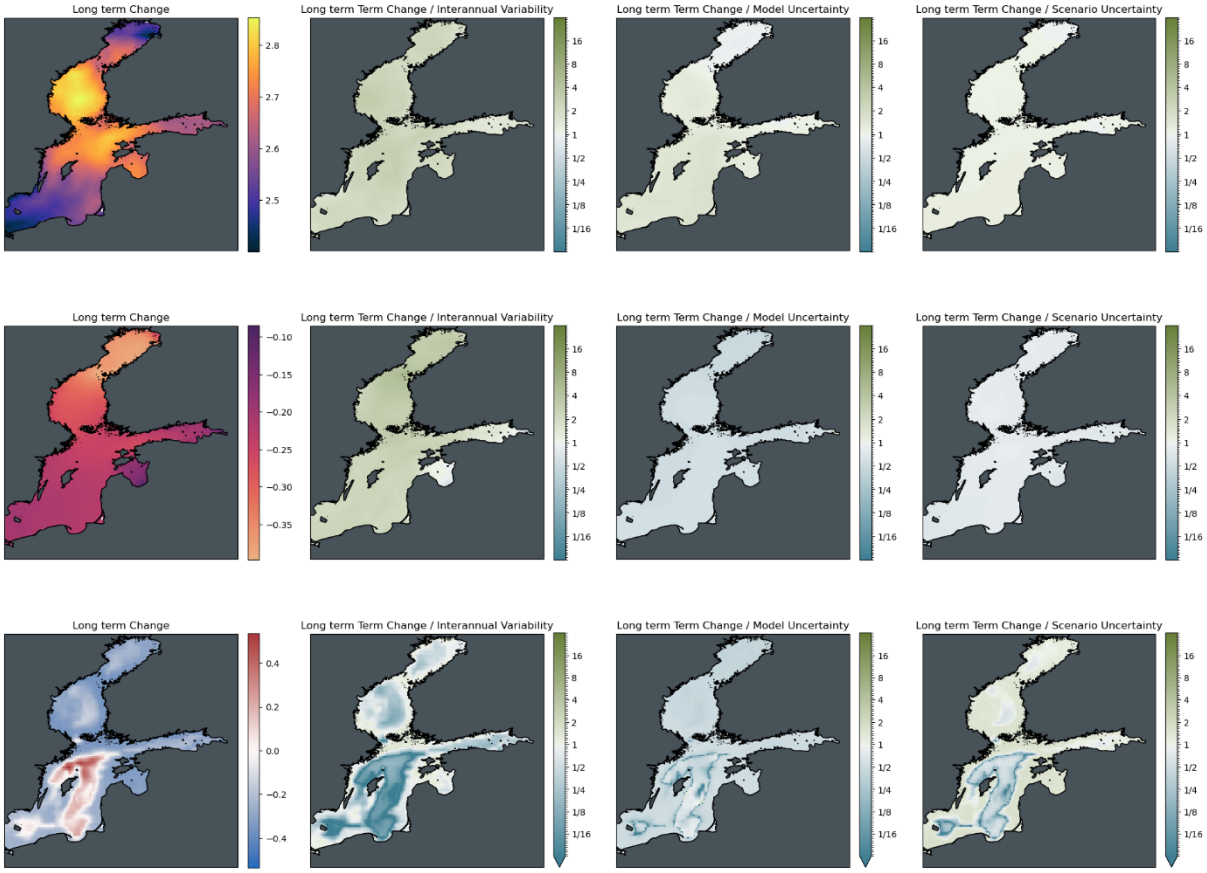

Figure 26 Significance of long-term changes in the Baltic Sea against three sources of uncertainty under scenario SSP2-4.5 for three ecosystem pressures. From left to right: changes between long-term conditions (2081-2100 mean) and present-day conditions (1995-2014); changes relative to internal variability; changes relative to model uncertainty; changes relative to scenario uncertainty. Top to bottom: Surface Temperature [K]; surface pH; bottom dissolved oxygen [ml/l].

3.2.5 Chile

For the area of the Chilean Pacific the evolution of the three analysed ecosystem pressures is once again qualitatively similar to global trends except for the deoxygenation where there appears to be no difference at basin scale in between the three mitigation pathways analysed. In addition, warming appears to be a little weaker (up to 3 degrees) compared to global changes (up to 4 degrees, (Kwiatkowski et al., 2020)).

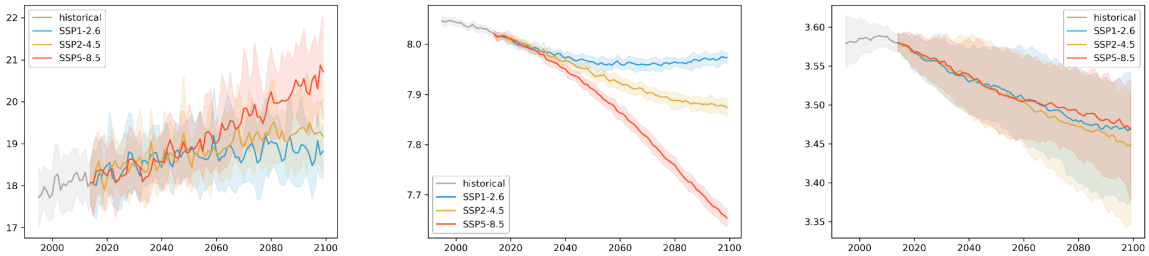

Figure 27 Time series of surface temperature (C), pH and bottom oxygen [ml/l] for the Chilean Pacific over the historical time slice and the three scenarios. Full lines show the ensemble, shaded areas show the ensemble spread based on the 2.5 and 97.5 percentiles of the model distribution.

The spatial patterns of these trends display a clear coastal gradient with increased warming and reduced acidification towards the coast compared to offshore waters, most likely caused by a reduced upwelling, a process that dominates the abiotic and biogeochemical characteristics of these waters. Warming trends, however, only clearly emerged from interannual variability and model uncertainty by the end of century. An exception was the waters at the western edge of the domain towards the open Pacific. Acidification trends were significant with respect to both sources of uncertainty at both time slices. Differences in between the scenarios for warming and acidification are still comparatively small compared to the trends at mid-century (roughly ¼ of the trend for warming and ½ for acidification) while they become substantial towards 2100 (1.5 times the trend for warming and about 3 times for acidification). Deoxygenation was projected to occur across nearly all of the domain (except for the north-western edge at both time slices) and significant with respect to interannual variability. These trends are, however, subject to substantial model uncertainty diminishing the confidence of these results. The different greenhouse gas emission pathways appear to have a neglectable impact on deoxygenation in this domain.

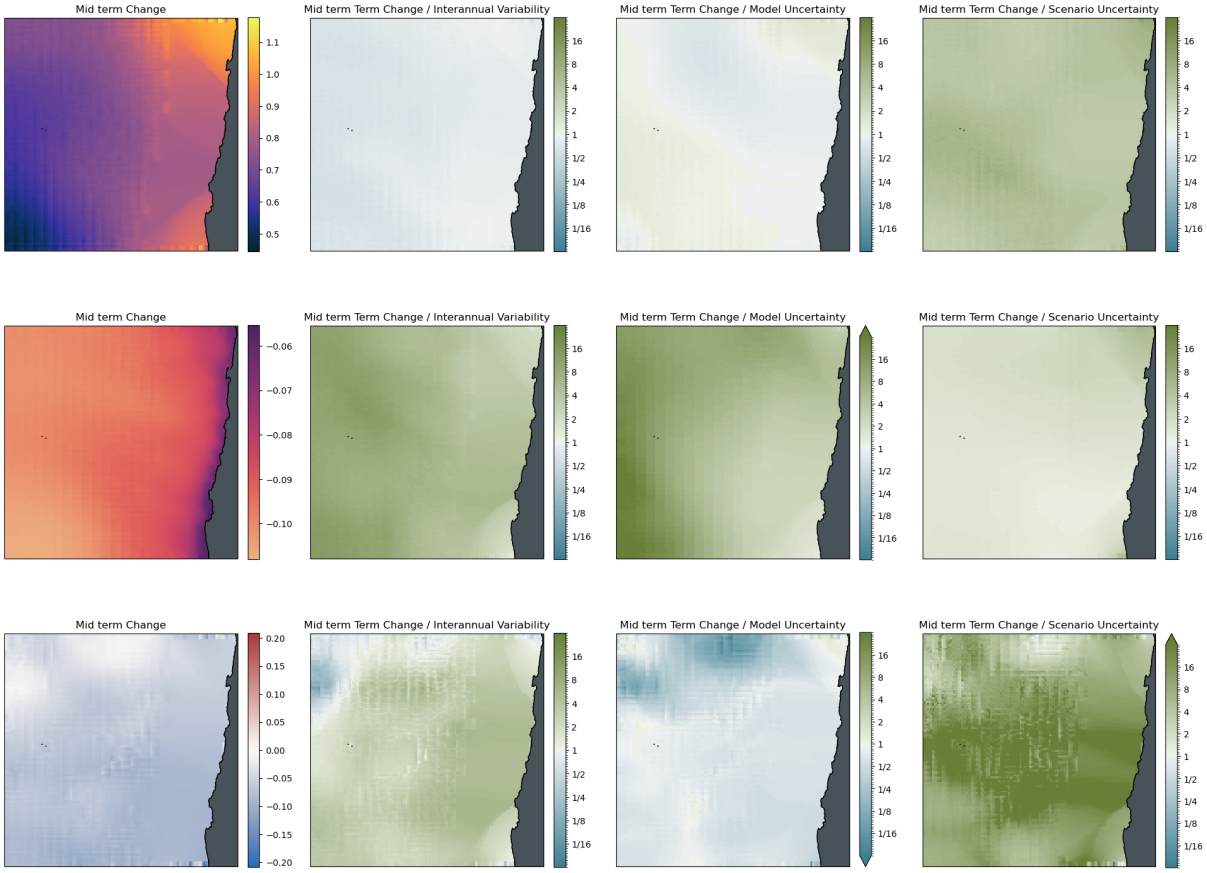

Figure 28 Significance of mid-term changes in the Chilean Pacific against three sources of uncertainty under scenario SSP2-4.5 for three ecosystem pressures. From left to right: changes between long-term conditions (2081-2100 mean) and present-day conditions (1995-2014); changes relative to internal variability; changes relative to model uncertainty; changes relative to scenario uncertainty. Top to bottom: Surface Temperature [K]; surface pH; bottom dissolved oxygen [ml/l].

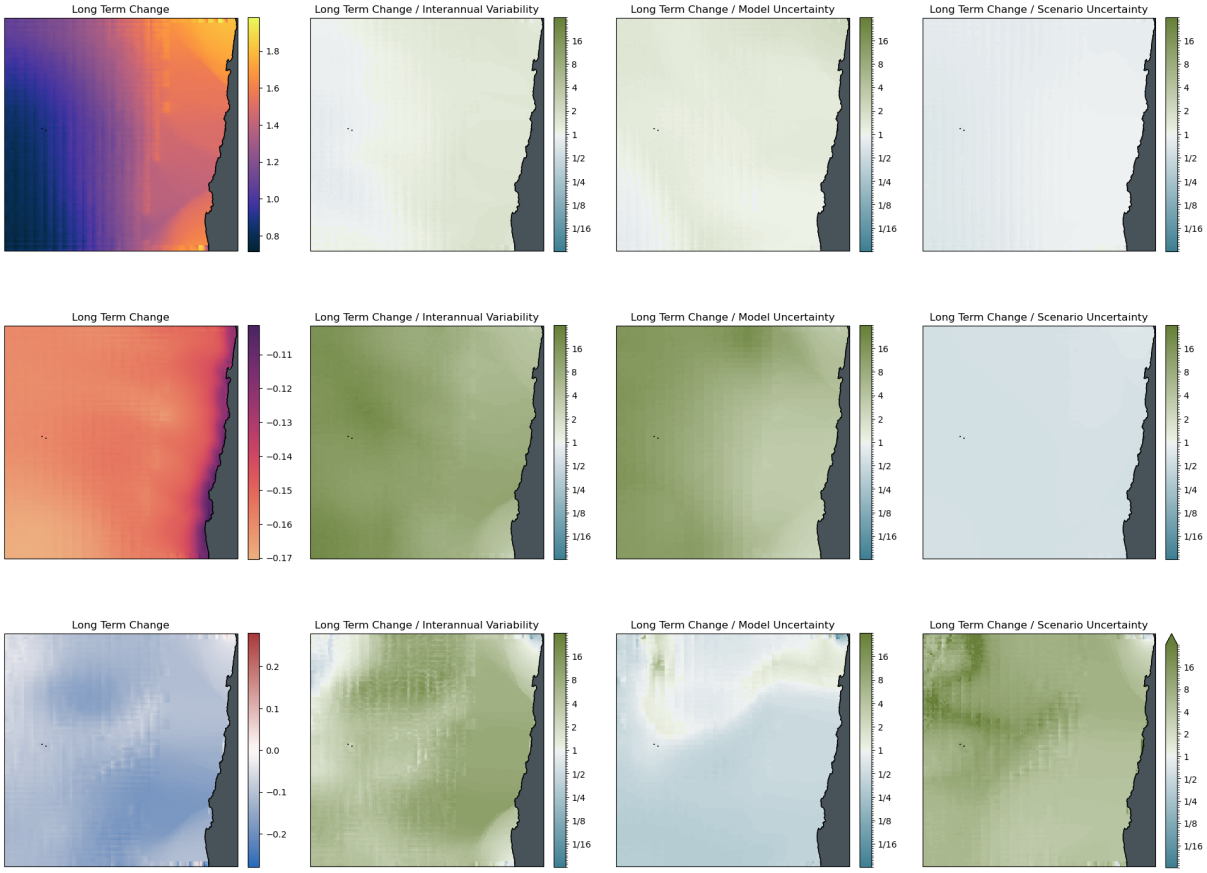

Figure 29 Significance of long-term changes in the Chilean Pacific against three sources of uncertainty under scenario SSP2-4.5 for three ecosystem pressures. From left to right: changes between long-term conditions (2081-2100 mean) and present-day conditions (1995-2014); changes relative to internal variability; changes relative to model uncertainty; changes relative to scenario uncertainty. Top to bottom: Surface Temperature [K]; surface pH; bottom dissolved oxygen [ml/l].

4. Summary

The assessment and analysis presented within this report provides an overview of the performance (skill) of statistically downscaled ensemble datasets for regional physical and biogeochemical habitat conditions originally published in D1.2 “Ensemble Data Set of Key Model Variables”. The skill of these projections was assessed via comparison to observations and the original ESM simulations. This report also present analyses of three key sources of uncertainties related to ensemble projections.

There was a clear improvement in model skill (Section 3.1) of the downscaled products compared to the original CMs and ESMs that were at the base of the bias adjustments and statistical downscaling. Nearly all of the bias of the original simulations was removed across all quantiles of the model data distributions leading to values of mean and standard deviations of the seasonal spatial climatologies that match those observed and reported in the WOA climatologies. In addition, inter-model differences in skill were strongly reduced in this process. The direct validation against the CORA 5.2 dataset for surface temperature was encouraging in terms of performance, particularly considering the limitations that inherently exist for uninitialized systems such as CMs and ESMs in matching particular phases of interannual variability.

The uncertainty analysis has highlighted some interesting and important features of the ensemble datasets. In general, the regional, basin-scale trends produced by the ensemble largely, qualitatively reflected the global changes but, importantly, were not distributed homogeneously across the regions. An exception to this was the Baltic Sea, a largely enclosed sea that is under much stronger influence than the other regions from coastal (watershed) processes. Warming was projected across virtually all domains but only fully emerged from the background uncertainties at the end of the century, except for the Mediterranean Sea. Our analyses revealed that warming emerged from projection uncertainties by the mid-century time slice, confirming that the Mediterranean Sea is a hotspot of global climate change. Ocean Acidification trends were fully significant at both the mid- and late-century time slices and show neglectable model uncertainty and interannual variability (with the exception of the Baltic Sea). On the contrary, trends in deoxygenation were much less clear and displayed high model uncertainty. Deoxygenation is a more complex process indirectly affected by anthropogenic greenhouse gas emissions via chemical (solubility) and biological (production and respiration) pathways.

Differences in IPCC RCP scenarios were generally detectable by mid-century, but fully apparent towards the end of the century, underlining the importance of consistent actions related to policies of climate change mitigation and adaptation.

Indexes

Index of figures

Index of tables

References

Boucher, O., Servonnat, J., Albright, A.L., Aumont, O., Balkanski, Y., Bastrikov, V., Bekki, S., Bonnet, R., Bony, S., Bopp, L., Braconnot, P., Brockmann, P., Cadule, P., Caubel, A., Cheruy, F., Codron, F., Cozic, A., Cugnet, D., D'Andrea, F., Davini, P., de Lavergne, C., Denvil, S., Deshayes, J., Devilliers, M., Ducharne, A., Dufresne, J.-L., Dupont, E., Éthé, C., Fairhead, L., Falletti, L., Flavoni, S., Foujols, M.-A., Gardoll, S., Gastineau, G., Ghattas, J., Grandpeix, J.-Y., Guenet, B., Guez, E., Lionel, Guilyardi, E., Guimberteau, M., Hauglustaine, D., Hourdin, F., Idelkadi, A., Joussaume, S., Kageyama, M., Khodri, M., Krinner, G., Lebas, N., Levavasseur, G., Lévy, C., Li, L., Lott, F., Lurton, T., Luyssaert, S., Madec, G., Madeleine, J.-B., Maignan, F., Marchand, M., Marti, O., Mellul, L., Meurdesoif, Y., Mignot, J., Musat, I., Ottlé, C., Peylin, P., Planton, Y., Polcher, J., Rio, C., Rochetin, N., Rousset, C., Sepulchre, P., Sima, A., Swingedouw, D., Thiéblemont, R., Traore, A.K., Vancoppenolle, M., Vial, J., Vialard, J., Viovy, N., Vuichard, N., 2020. Presentation and Evaluation of the IPSL-CM6A-LR Climate Model. J. Adv. Model. Earth Syst. 12, e2019MS002010. https://doi.org/10.1029/2019MS002010

Cherchi, A., Fogli, P.G., Lovato, T., Peano, D., Iovino, D., Gualdi, S., Masina, S., Scoccimarro, E., Materia, S., Bellucci, A., Navarra, A., 2019. Global Mean Climate and Main Patterns of Variability in the CMCC-CM2 Coupled Model. J. Adv. Model. Earth Syst. 11, 185–209. https://doi.org/10.1029/2018MS001369

Drenkard, E.J., Stock, C., Ross, A.C., Dixon, K.W., Adcroft, A., Alexander, M., Balaji, V., Bograd, S.J., Butenschön, M., Cheng, W., Curchitser, E., di Lorenzo, E., Dussin, R., Haynie, A.C., Harrison, M., Hermann, A., Hollowed, A., Holsman, K., Holt, J., Jacox, M.G., Jang, C.J., Kearney, K.A., Muhling, B.A., Buil, M.P., Saba, V., Sandø, A.B., Tommasi, D., Wang, M., 2021. Next-generation regional ocean projections for living marine resource management in a changing climate. ICES J. Mar. Sci. https://doi.org/10.1093/icesjms/fsab100

Drévillon, M., LeLlouche, J.-M., Régnier, C., Garric, G., Bricaud, C., Hernandez, O., Bourdallé-Badie, R., 2022. QUID For Global Ocean Reanalysis Products GLOBAL-REANALYSIS-PHY-001-030. Copernicus Marine Enviroment Monitoring Service, Toulouse.

Dunne, J.P., Horowitz, L.W., Adcroft, A.J., Ginoux, P., Held, I.M., John, J.G., Krasting, J.P., Malyshev, S., Naik, V., Paulot, F., Shevliakova, E., Stock, C.A., Zadeh, N., Balaji, V., Blanton, C., Dunne, K.A., Dupuis, C., Durachta, J., Dussin, R., Gauthier, P.P.G., Griffies, S.M., Guo, H., Hallberg, R.W., Harrison, M., He, J., Hurlin, W., McHugh, C., Menzel, R., Milly, P.C.D., Nikonov, S., Paynter, D.J., Ploshay, J., Radhakrishnan, A., Rand, K., Reichl, B.G., Robinson, T., Schwarzkopf, D.M., Sentman, L.T., Underwood, S., Vahlenkamp, H., Winton, M., Wittenberg, A.T., Wyman, B., Zeng, Y., Zhao, M., 2020. The GFDL Earth System Model Version 4.1 (GFDL-ESM 4.1): Overall Coupled Model Description and Simulation Characteristics. J. Adv. Model. Earth Syst. 12, e2019MS002015. https://doi.org/10.1029/2019MS002015

Frölicher, T.L., Rodgers, K.B., Stock, C.A., Cheung, W.W.L., 2016. Sources of uncertainties in 21st century projections of potential ocean ecosystem stressors. Glob. Biogeochem. Cycles 30, 1224–1243. https://doi.org/10.1002/2015GB005338

Garcia, H., Weathers, K., Paver, C., Smolyar, I., Boyer, T., Locarnini, M., Zweng, M., Mishonov, A., Baranova, O., Seidov, D., Reagan, J., 2019. World Ocean Atlas 2018, Volume 3: Dissolved Oxygen, Apparent Oxygen Utilization, and Dissolved Oxygen Saturation.

Gupta, H.V., Kling, H., Yilmaz, K.K., Martinez, G.F., 2009. Decomposition of the mean squared error and NSE performance criteria: Implications for improving hydrological modelling. J. Hydrol. 377, 80–91. https://doi.org/10.1016/j.jhydrol.2009.08.003

Gustafsson, E., Gustafsson, B.G., 2020. Future acidification of the Baltic Sea – A sensitivity study. J. Mar. Syst. 211, 103397. https://doi.org/10.1016/j.jmarsys.2020.103397

Hawkins, E., Sutton, R., 2009. The Potential to Narrow Uncertainty in Regional Climate Predictions. Bull. Am. Meteorol. Soc. 90, 1095–1107. https://doi.org/10.1175/2009BAMS2607.1

IPCC, 2021. Climate Change 2021: The Physical Science Basis. Contribution of Working Group I to the Sixth Assessment Report of the Intergovernmental Panel on Climate Change, in: Masson-Delmotte, V., Zhai, P., Pirani, A., Connors, S.I., Péan, C., Berger, S.., Caud, N.., Chen, IY., Goldfarb, L., Gomis, M.I., Huang, M., Leizzel, K., Lonnoy, E., Matthews, J.B.R., Maycock, T.K., Waterfield, T., Yelekçi, O., Yu, R., Zhou, B. (Eds.), . IPCC, Cambridge, United Kingdom and New York, NY, USA, p. 2391 pp.

Kwiatkowski, L., Torres, O., Bopp, L., Aumont, O., Chamberlain, M., Christian, J.R., Dunne, J.P., Gehlen, M., Ilyina, T., John, J.G., Lenton, A., Li, H., Lovenduski, N.S., Orr, J.C., Palmieri, J., Santana-Falcón, Y., Schwinger, J., Séférian, R., Stock, C.A., Tagliabue, A., Takano, Y., Tjiputra, J., Toyama, K., Tsujino, H., Watanabe, M., Yamamoto, A., Yool, A., Ziehn, T., 2020. Twenty-first century ocean warming, acidification, deoxygenation, and upper-ocean nutrient and primary production decline from CMIP6 model projections. Biogeosciences 17, 3439–3470. https://doi.org/10.5194/bg-17-3439-2020

Liu, D., 2020. A rational performance criterion for hydrological model. J. Hydrol. 590, 125488. https://doi.org/10.1016/j.jhydrol.2020.125488

Locarnini, M., Mishonov, A., Baranova, O., Boyer, T., Zweng, M., Garcia, H., Reagan, J., Seidov, D., Weathers, K., Paver, C., Smolyar, I., 2018. World Ocean Atlas 2018, Volume 1: Temperature.

Lovato, T., Peano, D., Butenschön, M., Materia, S., Iovino, D., Scoccimarro, E., Fogli, P.G., Cherchi, A., Bellucci, A., Gualdi, S., Masina, S., Navarra, A., 2022. CMIP6 Simulations With the CMCC Earth System Model (CMCC-ESM2). J. Adv. Model. Earth Syst. 14, e2021MS002814. https://doi.org/10.1029/2021MS002814

Mauritsen, T., Bader, J., Becker, T., Behrens, J., Bittner, M., Brokopf, R., Brovkin, V., Claussen, M., Crueger, T., Esch, M., Fast, I., Fiedler, S., Fläschner, D., Gayler, V., Giorgetta, M., Goll, D.S., Haak, H., Hagemann, S., Hedemann, C., Hohenegger, C., Ilyina, T., Jahns, T., Jimenéz-de-la-Cuesta, D., Jungclaus, J., Kleinen, T., Kloster, S., Kracher, D., Kinne, S., Kleberg, D., Lasslop, G., Kornblueh, L., Marotzke, J., Matei, D., Meraner, K., Mikolajewicz, U., Modali, K., Möbis, B., Müller, W.A., Nabel, J.E.M.S., Nam, C.C.W., Notz, D., Nyawira, S.-S., Paulsen, H., Peters, K., Pincus, R., Pohlmann, H., Pongratz, J., Popp, M., Raddatz, T.J., Rast, S., Redler, R., Reick, C.H., Rohrschneider, T., Schemann, V., Schmidt, H., Schnur, R., Schulzweida, U., Six, K.D., Stein, L., Stemmler, I., Stevens, B., von Storch, J.-S., Tian, F., Voigt, A., Vrese, P., Wieners, K.-H., Wilkenskjeld, S., Winkler, A., Roeckner, E., 2019. Developments in the MPI-M Earth System Model version 1.2 (MPI-ESM1.2) and Its Response to Increasing CO2. J. Adv. Model. Earth Syst. 11, 998–1038. https://doi.org/10.1029/2018MS001400

Nash, J.E., Sutcliffe, J.V., 1970. River flow forecasting through conceptual models part I — A discussion of principles. J. Hydrol. 10, 282–290. https://doi.org/10.1016/0022-1694(70)90255-6

O'Neill, B.C., Tebaldi, C., van Vuuren, D., Eyring, V., Friedlingstein, P., Hurtt, G., Knutti, R., Kriegler, E., Lamarque, J.-F., Lowe, J., Meehl, J., Moss, R., Riahi, K., Sanderson, B.M., 2016. The Scenario Model Intercomparison Project (ScenarioMIP) for CMIP6. Geosci. Model Dev. Discuss. 1–35. https://doi.org/10.5194/gmd-2016-84

Perruche, C., Szczypta, C., Paul, J., Drévillon, M., 2019. QUID for Global Ocean Biogeochemistry Hindcast. GLOBAL_REANALYSIS_BIO_001_029. Copernicus Marine Enviroment Monitoring Service, Toulouse.

Szekely, T., Gourrion, J., Pouliquen, S., Reverdin, G., 2019. The CORA 5.2 dataset for global in situ temperature and salinity measurements: data description and validation. Ocean Sci. 15, 1601–1614. https://doi.org/10.5194/os-15-1601-2019

Taylor, K.E., 2001. Summarizing multiple aspects of model performance in a single diagram. J. Geophys. Res.-Atmospheres 106, 7183–7192. https://doi.org/10.1029/2000JD900719